SCIENCE CHINA PRESS

SCIENCE CHINA Life Sciences
life.scichina.com link.springer.com
https://doi.org/10.1007/s11427-023-2451-3

RESEARCH PAPER

CRL2^{APPBP2}-mediated TSPYL2 degradation counteracts human mesenchymal stem cell senescence

Daoyuan Huang[1,3†], Qian Zhao[1,3†], Kuan Yang[5,7,10†], Jinghui Lei[1,3], Ying Jing[1,3], Hongyu Li[5,11], Chen Zhang[9], Shuai Ma[4,6,8], Shuhui Sun[4,6,8], Yusheng Cai[4,6,8], Guibin Wang[12], Jing Qu[2,5,6,8], Weiqi Zhang[5,7,8,10*], Si Wang[1,3,9*] & Guang-Hui Liu[1,3,4,5,6,8*]

[1]Advanced Innovation Center for Human Brain Protection, National Clinical Research Center for Geriatric Disorders, Xuanwu Hospital Capital Medical University, Beijing 100053, China;
[2]State Key Laboratory of Stem Cell and Reproductive Biology, Institute of Zoology, Chinese Academy of Sciences, Beijing 100101, China;
[3]Aging Translational Medicine Center, International Center for Aging and Cancer, Beijing Municipal Geriatric Medical Research Center, Xuanwu Hospital, Capital Medical University, Beijing 100053, China;
[4]State Key Laboratory of Membrane Biology, Institute of Zoology, Chinese Academy of Sciences, Beijing 100101, China;
[5]University of Chinese Academy of Sciences, Beijing 100049, China;
[6]Beijing Institute for Stem Cell and Regenerative Medicine, Beijing, 100101, China;
[7]CAS Key Laboratory of Genomic and Precision Medicine, Beijing Institute of Genomics and China National Center for Bioinformation, Chinese Academy of Sciences, Beijing 100101, China;
[8]Institute for Stem Cell and Regeneration, CAS, Beijing 100101, China;
[9]The Fifth People's Hospital of Chongqing, Chongqing 400062, China;
[10]Sino-Danish College, University of Chinese Academy of Sciences, Beijing, 101408, China;
[11]National Laboratory of Biomacromolecules, CAS Center for Excellence in Biomacromolecules, Institute of Biophysics, Chinese Academy of Sciences, Beijing, 100101, China;
[12]State Key Laboratory of Proteomics, Beijing Proteome Research Center, National Center for Protein Sciences (Beijing), Beijing Institute of Lifeomics, Beijing 102206, China

†Contributed equally to this work
*Corresponding authors (Weiqi Zhang, email: zhangwq@big.ac.cn; Si Wang, email: wangsi@xwh.ccmu.edu.cn; Guang-Hui Liu, email: ghliu@ioz.ac.cn)

Received 30 June 2023; Accepted 13 September 2023; Published online 7 December 2023

Cullin-RING E3 ubiquitin ligases (CRLs), the largest family of multi-subunit E3 ubiquitin ligases in eukaryotic cells, represent core cellular machinery for executing protein degradation and maintaining proteostasis. Here, we asked what roles Cullin proteins play in human mesenchymal stem cell (hMSC) homeostasis and senescence. To this end, we conducted a comparative aging phenotype analysis by individually knocking down Cullin members in three senescence models: replicative senescent hMSCs, Hutchinson-Gilford Progeria Syndrome hMSCs, and Werner syndrome hMSCs. Among all family members, we found that *CUL2* deficiency rendered hMSCs the most susceptible to senescence. To investigate CUL2-specific underlying mechanisms, we then applied CRISPR/Cas9-mediated gene editing technology to generate *CUL2*-deficient human embryonic stem cells (hESCs). When we differentiated these into hMSCs, we found that *CUL2* deletion markedly accelerates hMSC senescence. Importantly, we identified that CUL2 targets and promotes ubiquitin proteasome-mediated degradation of TSPYL2 (a known negative regulator of proliferation) through the substrate receptor protein APPBP2, which in turn downregulates one of the canonical aging marker-P21$^{waf1/cip1}$, and thereby delays senescence. Our work provides important insights into how CRL2^{APPBP2}-mediated TSPYL2 degradation counteracts hMSC senescence, providing a molecular basis for directing intervention strategies against aging and aging-related diseases.

Cullins | stem cell | senescence | aging | proteostasis | ubiquitination | APPBP2 | TSPYL2

INTRODUCTION

Loss of proteostasis is a major characteristic of aging and an important contributor to organismal dysfunction (Bao et al., 2023; López-Otín et al., 2023; Noormohammadi et al., 2018). At a cellular level, abnormal protein folding and toxic protein accumulation cause cellular damage that exacerbates tissue dysfunction during aging (Hipp et al., 2019). Two principal protein degradation systems, namely the ubiquitin-proteasome system (UPS) and the autophagy-lysosome system (ALS), clear abnormal proteins (Dikic, 2017; Hipp et al., 2019; Zhang et al., 2022b), but the activity of these two systems decreases with age, instigating an imbalance in protein homeostasis and subsequently triggering an array of degenerative diseases. However, the precise molecular mechanism responsible for the disruption of proteostasis in human cells and organs remains largely elusive.

Within the ubiquitin-proteasome system, the binding of ubiquitin to target proteins is coordinated by several synergistic components, including ubiquitin-activating enzyme (E1), ubiquitin-binding enzyme (E2) and ubiquitin ligase (E3) (Hershko and Ciechanover, 1992; Scheffner et al., 1995). Among them, the E3 ligases are considered to play the most direct role in substrate recognition (Scheffner et al., 1995). Cullin-RING E3 ubiquitin ligases (CRLs), which represent the most extensive family of multi-subunit E3 ubiquitin ligases in eukaryotic cells, are estimated to degrade approximately 20% of intracellular proteins destined for degradation by the UPS (Soucy et al., 2009). The Cullin protein family, consisting of eight mammalian members (CUL1, CUL2, CUL3, CUL4A, CUL4B, CUL5, CUL7, and CUL9/PARC), function as the core scaffold in CRLs (Sarikas et al., 2011). Cullin family proteins have been studied in various biological contexts, spanning cell cycle regulation, DNA replication, and development (Sarikas et al., 2011). However, the majority of these studies have focused on human tumor cell lines

and mice, limiting insight into their physiological role in humans. Here, we considered that human mesenchymal stem cells (hMSCs) serve as the source of organismal homeostasis and regeneration, and that hMSC senescence is a central contributor to organ and organismal aging. On this basis, we set out to examine the role of CRLs hMSC senescence as a gateway for understanding their roles in aging and exploring means to delay aging and aging-related disorders.

First, via screening with genetic manipulation of all members of Cullin family, we discovered that CUL2 plays a vital role in delaying senescence of replicative senescent (RS) hMSCs, Werner syndrome (WS) hMSCs, and Hutchinson-Gilford Progeria Syndrome (HGPS) hMSCs models. Through integrated analysis of interactome, transcriptome, and quantitative proteome sequencing, we found that $CRL2^{APPBP2}$ delays hMSC senescence by targeting the degradation of TSPYL2, an anti-proliferative factor that promotes P21 expression. We further elucidated the molecular mechanism underlying the regulation of aging and homeostasis maintenance in hMSCs by CUL2 through the ubiquitin-proteasome pathway, and suggest intervention strategies with potential for delaying the aging process.

RESULTS

Loss of CUL2 renders hMSCs susceptible to senescence

To identify Cullin family members impacting on regulation of cellular senescence in hMSCs, we infected RS hMSCs, HGPS hMSCs and WS hMSCs with CRISPR/Cas9-mediated knockout lentiviruses of Cullin family members, including CUL1, CUL2, CUL3, CUL4A, CUL4B, CUL5, CUL7, and CUL9/PARC, and control lentivirus (sg-NC), respectively (Figure 1A). We found that knockdown of CUL2 by its three independent sgRNAs in all three senescent mesenchymal cell models (RS hMSCs, HGPS hMSCs and WS hMSCs) resulted in an increased senescence-associated β-galactosidase (SA-β-Gal)-positive cells (Figure 1B–E). Moreover, CUL2 knockdown also led to compromised clonal expansion capacity (Figure 1F), suggesting accelerated cellular senescence in hMSCs upon CUL2 silencing. Consistently, knockdown of CUL2 by using shRNAs against *CUL2* also resulted in an expedited progression of senescence in hMSCs, as evidenced by an increase in SA-β-Gal-positive cells and decreased clonal expansion capacity (Figure 1G–I). These results suggest that of all Cullin members, CUL2 is the most important for preventing hMSC senescence.

CUL2 deletion accelerates the senescence of hMSCs

To examine whether and how CUL2 acts as a geroprotector against hMSC senescence, we applied CRISPR/Cas9-mediated gene editing technology to obtain *CUL2*-deletion in human embryonic stem cells (hESCs). Gene editing with *CUL2* sgRNA resulted in an insertion of one base pair (G/C) within the exon 3, and Western blotting result also showed the absence of CUL2 protein expression (Figure S1A and B in Supporting Information). We found that the expression levels of pluripotency markers in $CUL2^{-/-}$ hESCs were similar to those in $CUL2^{+/+}$ hESCs (Figure S1C in Supporting Information) and that the potential for germ layer differentiation was well maintained in $CUL2^{-/-}$ hESCs (Figure S1D in Supporting Information). Furthermore, *CUL2* deletion exhibited no impact on cell karyotype and genome integrity, as demonstrated by both karyotype and copy number variation (CNV) analysis (Figure S1E and F in Supporting Information). In addition, based on immunofluorescence analysis, the loss of CUL2 did not compromise cell proliferation (Figure S1G in Supporting Information). Collectively, these findings imply that *CUL2* may not be necessary for the self-renewal and maintenance of pluripotency in hESCs.

Next, differentiation of $CUL2^{+/+}$ and $CUL2^{-/-}$ hESCs into hMSCs was conducted (Figure 2A). By using Western blotting analysis, we first confirmed the successful deletion of CUL2 protein in $CUL2^{-/-}$ hMSCs (Figure 2B). Both $CUL2^{+/+}$ and $CUL2^{-/-}$ hMSCs exhibited comparable expression levels of classical hMSC markers, including CD73, CD90, and CD105 (Figure S2A in Supporting Information). Similar to $CUL2^{+/+}$ hMSCs, $CUL2^{-/-}$ hMSCs were successfully differentiated into chondrocytes, osteoblasts, and adipocytes (Figure S2B–D in Supporting Information), suggesting that differentiation potential is not impaired by CUL2 deficiency. Furthermore, CNV analysis showed that *CUL2* deletion did not affect the genomic integrity of hMSCs (Figure S2E in Supporting Information).

Consistent with previous observations (Figure 1B–I), we found that *CUL2* deficiency also accelerated senescence in hESC-derived hMSCs, manifested as reduced proliferative capacity, including decreased proportion of Ki67-positive cells, a decline in the proportion of S-phase cells, and reduced clonal expansion ability (Figure 2C–F), and an increase proportion of SA-β-Gal-positive cells relative to $CUL2^{+/+}$ hMSCs (Figure 2G). In addition, we detected changes in an array of senescence hallmarks associated with *CUL2* deficiency, including upregulation of classical aging-related markers *CDKN1A* (P21) and *CDKN2A* (P16), downregulation of *TMPO* (LAP2β), Lamin B1, H3K9me3, and HP1α (Figure 2H–M; Figure S2H in Supporting Information), as well as upregulation of SASP-related genes (*IL6*, *CXCL8*) in $CUL2^{-/-}$ hMSCs (Figure 2H). RNA-seq analysis demonstrated that *CUL2* deficiency resulted in downregulation of genes associated with cell cycle and proliferation (Figure S2F, G, and I in Supporting Information), consistent with the phenotypes observed in *CUL2*-deficient hMSCs. Additionally, we found increased DNA damage and reactive oxygen species (ROS) levels in $CUL2^{-/-}$ hMSCs (Figure 2N and O). Furthermore, by transplanting luciferase-labeled $CUL2^{+/+}$ and $CUL2^{-/-}$ hMSCs into immunodeficient mice's tibialis anterior muscle, we found a compromised *in vivo* stem cell retention capacity of $CUL2^{-/-}$ hMSCs relative to wildtype hMSCs (Figure 2P).

Importantly, when we reintroduced CUL2 protein into $CUL2^{-/-}$ hMSCs, the CUL2 deficiency-associated proliferation and senescence phenotypes were alleviated (Figure 2Q–S; Figure S2J in Supporting Information). Altogether, these findings suggest that CUL2 plays a geroprotective role in hMSCs.

Ectopic expression of CUL2 delays hMSC senescence

Given that expression of CUL2 is decreased in RS hMSCs (Figure 3A), we asked whether ectopic expression of CUL2 can rescue cellular senescence. By activating CUL2 expression by manipulating CRISPR activation, we observed that CUL2 expression alleviated the senescent phenotypes in RS hMSCs and HGPS hMSCs, as manifested by a reduced proportion of SA-β-Gal-positive cells and increased clonal expansion capacity (Figure 3B–G). Consistently, overexpression of CUL2 in RS hMSCs and

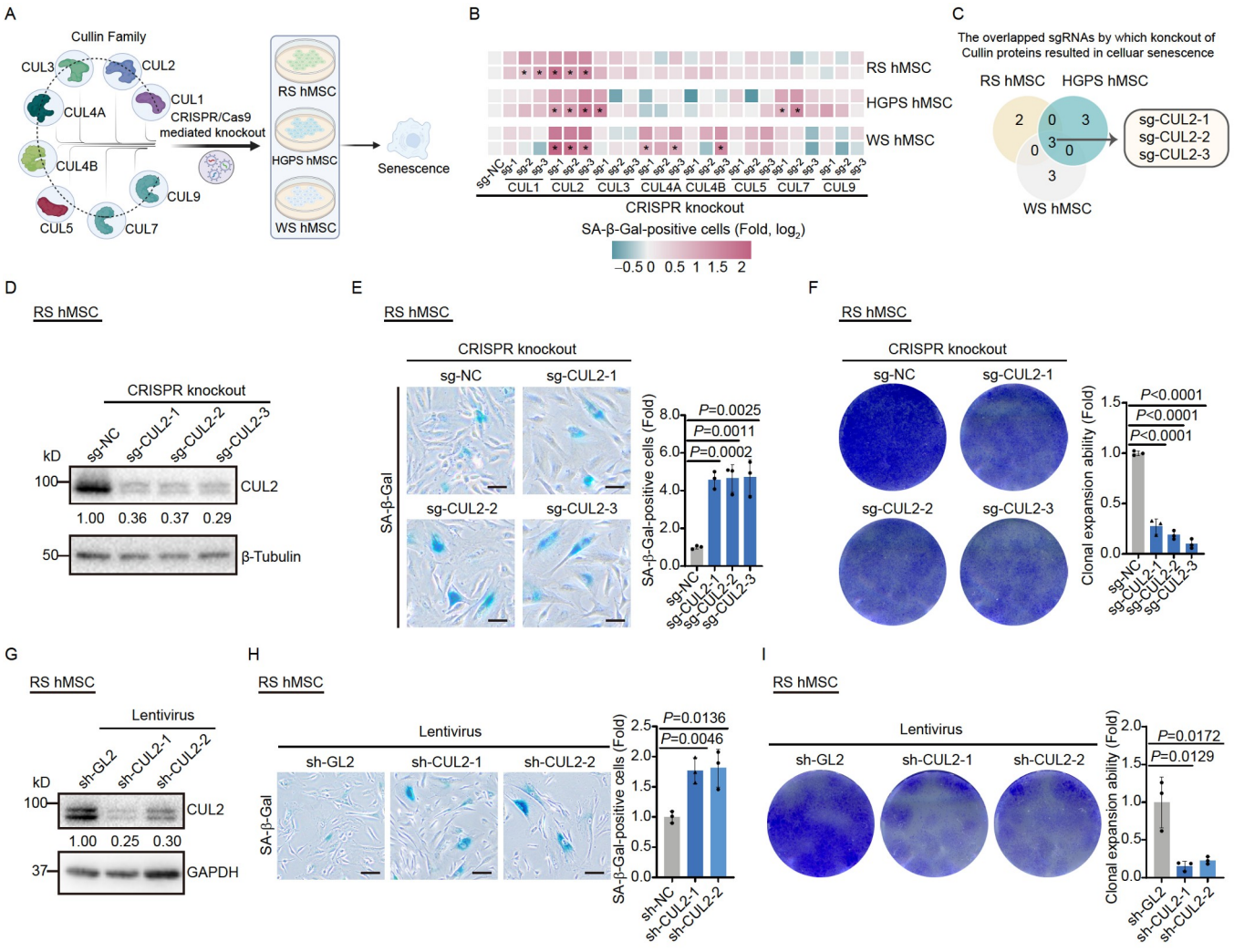

Figure 1. Silence of CUL2 promotes hMSC senescence. A, Screening strategy for studying the effect of Cullin family members on hMSC senescence. B, Heatmap showing the proportion of SA-β-Gal-positive cells in RS hMSCs, WS hMSCs and HGPS hMSCs after transducing lentiviruses expressing sgRNAs targeting each member of Cullin family. The color key ranging from green to pink represents $\log_2$ (fold change) values from low to high. *, $P<0.05$. C, Venn diagram showing the overlapped sgRNAs against the Cullin family members, by which knockout of Cullin proteins resulted in senescence of RS hMSC, HGPS hMSC, and WS hMSC. D, Western blotting detection of CUL2 expression in RS hMSC (P6) transduced with lentiviruses carrying CUL2-targeting sgRNAs or negative control sgRNA (sg-NC). β-Tubulin was used as loading control. E, SA-β-Gal staining analysis of RS hMSCs (P6) transduced with lentivirus carrying CUL2-targeting sgRNAs or sg-NC. Representative images were showed on the left. The proportion of SA-β-Gal-positive cells was quantified as fold changes (sg-CUL2 *vs.* sg-NC). $n=3$. Scale bars, 100 μm. F, Clonal expansion assay analysis of RS hMSCs (P6) transduced with lentivirus carrying CUL2-targeting sgRNAs or sg-NC. Representative images were showed on the left. Clonal expansion ability was quantified as fold changes (sg-CUL2 *vs.* sg-NC). $n=3$. G, Western blotting detection of CUL2 expression in RS hMSCs (P6) transduced with lentiviruses expressing sh-CUL2 or sh-GL2. H, SA-β-Gal staining analysis of RS hMSCs (P6) transduced with lentiviruses expressing sh-CUL2 or sh-GL2. Representative images were showed on the left. The proportion of SA-β-Gal-positive cells was quantified as fold changes (sh-CUL2 *vs.* sh-GL2). $n=3$. Scale bars, 100 μm. I, Clonal expansion assay analysis of RS hMSCs (P6) transduced with lentiviruses expressing sh-CUL2 or sh-GL2. Representative images are presented on the left. The data were quantified as fold changes (sh-CUL2 *vs.* sh-GL2). $n=3$. The data were analyzed by using two-tailed unpaired Student's *t*-test and are presented as means±SEM.

HGPS hMSCs also led to a decline in the proportion of SA-β-Gal-positive cells, along with an increase in cell proliferation, as demonstrated by increased Ki67-positive cells, and enhanced clonal expansion capacity (Figure 3H–N). In addition, CUL2 overexpression resulted in increased abundance of H3K9me3 (Figure 3O). These results demonstrated that ectopic expression of CUL2 attenuates hMSC senescence.

CUL2 regulates TSPYL2 protein stability through the ubiquitin proteasome pathway

The main function of CUL2 is to degrade downstream substrate proteins by assembling with Elongin B (EloB) and Elongin C (EloC), ROC1 and other substrate recognition receptors into a CRL2 E3 ubiquitin ligase (CRL2) (Hua and Vierstra, 2011). Thus, we next sought to identify which substrates are degraded by CRL2 in hMSC senescence. To achieve this, we conducted quantitative proteomic analysis, revealing 266 downregulated and 249 upregulated differentially expressed proteins upon CUL2 deletion (Figure 4A; Figure S3A–C in Supporting Information). Consistently, Gene Ontology (GO) analysis suggested that knockout of CUL2 impaired cell cycle processes (Figure 4B). Next, we sought to identify the genes whose protein levels were upregulated but mRNA levels were not upregulated in *CUL2*$^{-/-}$ hMSCs, as these would be candidate substrates for CRL2 (Figure 4C). Amongst these was Testis-Specific Y-Encoded-Like Protein 2 (TSPYL2), also known as Cell Division Autoantigen 1 (CDA1), recognized for its suppressive effects on both cell proliferation and

https://doi.org/10.1007/s11427-023-2451-3

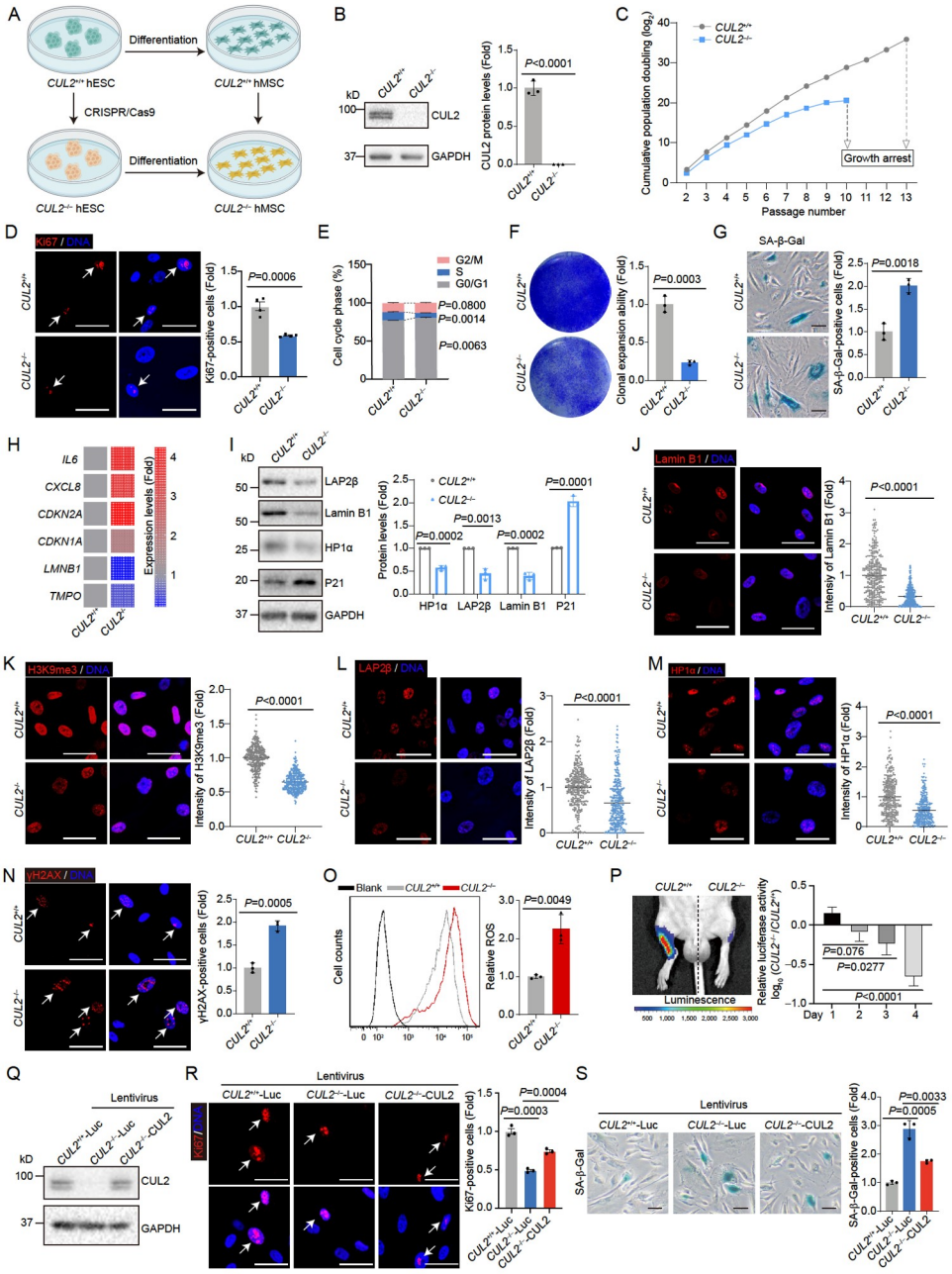

Figure 2. Loss of CUL2 accelerates hMSC senescence. A, A schematic diagram of hMSC differentiation from *CUL2*$^{+/+}$ hESC or *CUL2*$^{-/-}$ hESC. B, Western blotting detection of CUL2 in *CUL2*$^{+/+}$ and *CUL2*$^{-/-}$ hMSCs (P4). C, Growth curve analysis of *CUL2*$^{+/+}$ and *CUL2*$^{-/-}$ hMSCs. D, Immunofluorescence analysis of Ki67 in *CUL2*$^{+/+}$ and *CUL2*$^{-/-}$ hMSCs (P6). Representative images were showed on the left. The proportion of Ki67-positive cells was quantified as fold changes (*CUL2*$^{-/-}$ *vs.* *CUL2*$^{+/+}$). n=3. Scale bars, 50 μm. E, Cell cycle phase analysis was performed on *CUL2*$^{+/+}$ and *CUL2*$^{-/-}$ hMSCs (P6). F, Clonal expansion assay analysis of *CUL2*$^{+/+}$ and *CUL2*$^{-/-}$ hMSCs (P6). Representative images were showed on the left. Clonal expansion ability was quantified as fold changes (*CUL2*$^{+/+}$ *vs.* *CUL2*$^{-/-}$). n=3. G, SA-β-Gal staining analysis on *CUL2*$^{+/+}$ and *CUL2*$^{-/-}$ hMSCs (P6). Representative images were showed on the left. The proportion of SA-β-Gal-positive cells was quantified as fold changes (*CUL2*$^{-/-}$ *vs.* *CUL2*$^{+/+}$). n=3. Scale bars, 100 μm. H, Heatmap showing the mRNA level changes of *IL6*, *CXCL8*, *CDKN2A*, *CDKN1A*, *LMNB1*, and *TMPO* in *CUL2*$^{+/+}$ and *CUL2*$^{-/-}$ hMSCs (P9) by RT-qPCR. n=3. *GAPDH* was used as internal control. I, Western blot analysis for the expression of LAP2β, Lamin B1, HP1α, and P21 in *CUL2*$^{+/+}$ and *CUL2*$^{-/-}$ hMSCs (P9). GAPDH was used as loading control. J–M, Immunofluorescence analysis of Lamin B1 (J), H3K9me3 (K), LAP2β (L), HP1α (M) in *CUL2*$^{+/+}$ and *CUL2*$^{-/-}$ hMSCs (P6). Representative images were presented on the left. The intensity of fluorescence signal was quantified as fold changes (*CUL2*$^{-/-}$ *vs.* *CUL2*$^{+/+}$). Scale bars, 50 μm. N, Immunofluorescence analysis of γH2AX in *CUL2*$^{+/+}$ and *CUL2*$^{-/-}$ hMSCs (P6). Representative images were presented on the left. The proportion of γH2AX-positive cells was quantified as fold changes (*CUL2*$^{-/-}$ *vs.* *CUL2*$^{+/+}$). n=3. Scale bars, 50 μm. O, Cellular ROS levels were detected by flow cytometric analysis of H2DCFDA staining in *CUL2*$^{+/+}$ or *CUL2*$^{-/-}$ hMSCs (P6). The Relative ROS level was quantified as fold changes (*CUL2*$^{-/-}$ *vs.* *CUL2*$^{+/+}$). n=3. P, Luciferase (Luc) activity was measured by quantifying the photon flux emitted from the tibialis anterior muscles of nude mice that were implanted with *CUL2*$^{+/+}$ or *CUL2*$^{-/-}$ hMPCs (P5) expressing Luc. Luc activity was monitored on day 0, 1, 2, 3, and 4 following the implantation. Q, Western blotting analysis of CUL2 in *CUL2*$^{-/-}$ hMPCs (P6) that were transduced with lentiviruses carrying Luc or CUL2. GAPDH was used as loading control. R, Immunofluorescence analysis of Ki67 in *CUL2*$^{-/-}$ hMPCs (P6) that were transduced with lentiviruses expressing Luc or CUL2. Representative images were presented on the left. The proportion of Ki67-positive cells was quantified as fold changes (*CUL2*$^{-/-}$-Luc *vs.* *CUL2*$^{+/+}$-Luc, *CUL2*$^{-/-}$-CUL2 *vs.* *CUL2*$^{-/-}$-Luc). n=3. Scale bars, 50 μm. S, SA-β-Gal staining analysis of *CUL2*$^{-/-}$ hMPCs (P6) transduced with lentiviruses expressing either Luc or CUL2. Representative images were presented on the left. The proportion of SA-β-Gal-positive cells was quantified as fold changes (*CUL2*$^{-/-}$-Luc *vs.* *CUL2*$^{+/+}$-Luc, *CUL2*$^{-/-}$-CUL2 *vs.* *CUL2*$^{-/-}$-Luc). n=3. Scale bars, 100 μm. The data were analyzed by using two-tailed unpaired Student's *t*-test and are presented as means±SEM.

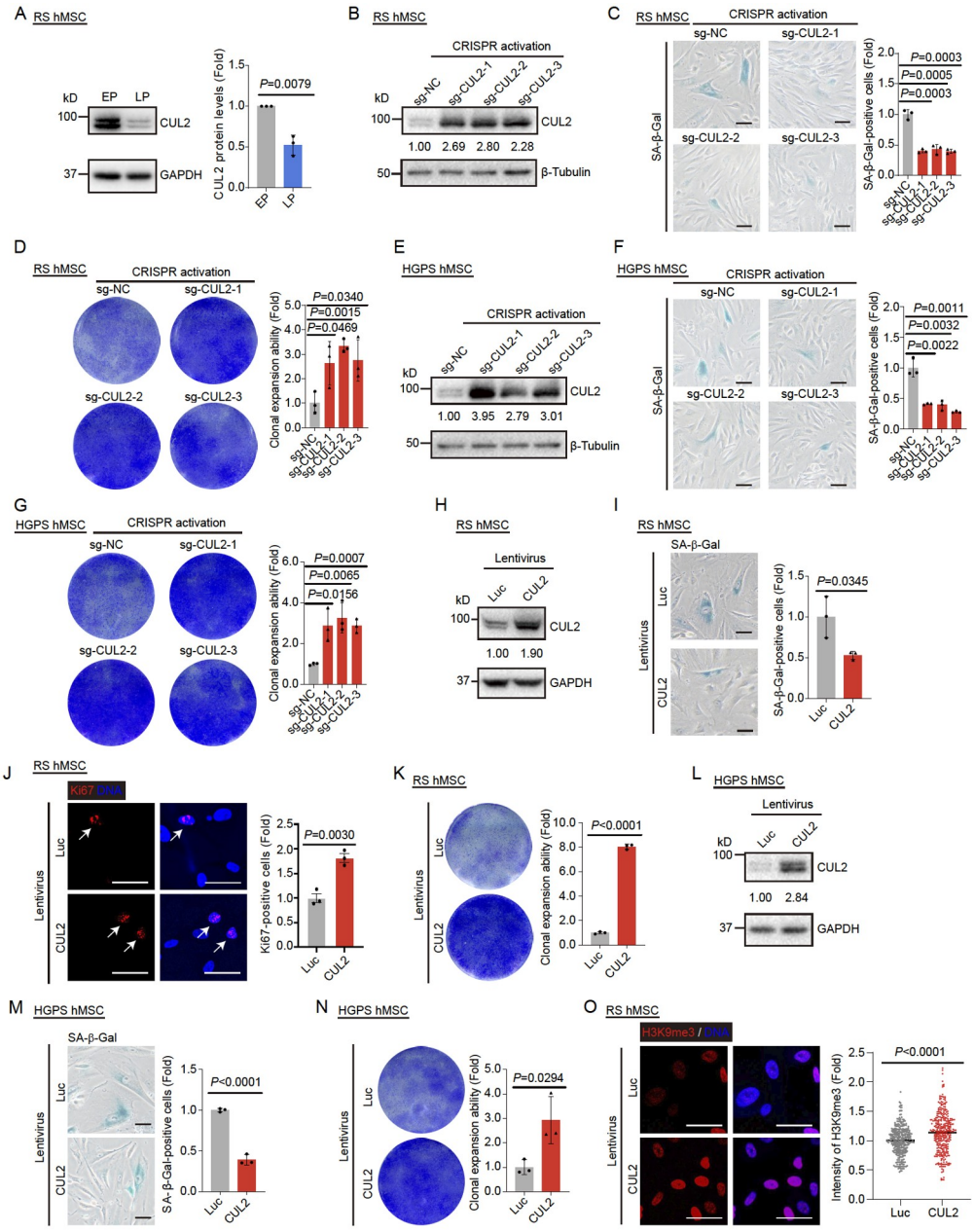

Figure 3. Ectopic expression of CUL2 counteracts hMSC senescence. A, Western blot analysis of CUL2 in RS hMSCs at different passages. Early passage (EP), P4; and late passage (LP), P12. GAPDH was used as loading control. B, Western blot analysis of CUL2 in RS hMSCs (P10) following transduction with CRISPR activation sgRNA targeting CUL2 (sg-CUL2) or negative control sgRNA (sg-NC). β-Tubulin was used as loading control. C, SA-β-Gal staining was performed on RS hMSCs (P10) following transduction with CRISPR activation sgRNA targeting CUL2 (sg-CUL2) or negative control sgRNA (sg-NC). Representative images were presented on the left. The proportion of SA-β-Gal-positive cells was quantified as fold changes (sg-CUL2 *vs.* sg-NC). $n=3$. Scale bars, 100 μm. D, A clonal expansion assay was conducted on RS hMSCs (P10) following transduction with CRISPR activation sgRNA targeting CUL2 (sg-CUL2) or negative control sgRNA (sg-NC). Representative images were presented on the left. Clonal expansion ability was quantified as fold changes (sg-CUL2 *vs.* sg-NC). $n=3$. E, Western blotting analysis for the expression of CUL2 in HGPS hMSCs (P6) following transduction with CRISPR activation sgRNA targeting CUL2 (sg-CUL2) or negative control sgRNA (sg-NC). β-Tubulin was used as loading control. F, SA-β-Gal staining was performed on HGPS hMSCs (P6) following transduction with CRISPR activation sgRNA targeting CUL2 (sg-CUL2) or negative control sgRNA (sg-NC). Representative images were presented on the left. The proportion of SA-β-Gal-positive cells was quantified as fold changes (sg-CUL2 *vs.* sg-NC). $n=3$. Scale bars, 100 μm. G, Clonal expansion assay analysis of HGPS hMSCs (P6) following transduction with CRISPR activation sgRNA targeting CUL2 (sg-CUL2) or negative control sgRNA (sg-NC). Representative images were presented on the left. The clonal expansion ability was quantified as fold changes (sg-CUL2 *vs.* sg-NC). $n=3$. H, Western blotting analysis of CUL2 expression in RS hMSCs (P8) following transduction with lentiviruses expressing Luc or CUL2. GAPDH was used as loading control. I, SA-β-Gal staining analysis on RS hMSCs (P8) following transduction with lentiviruses expressing either Luc or CUL2. Representative images were presented on the left. The proportion of SA-β-Gal-positive cells was quantified as fold changes (CUL2 *vs.* Luc). $n=3$. Scale bars, 100 μm. J, Immunofluorescence analysis of Ki67 in RS hMSCs (P8) following transduction with lentiviruses expressing Luc or CUL2. Representative images were presented on the left. The proportion of Ki67-positive cells was quantified as fold changes (CUL2 *vs.* Luc). $n=3$. Scale bars, 50 μm. K, Clonal expansion assay analysis of RS hMSCs (P8) following transduction with lentiviruses expressing Luc or CUL2. Representative images were presented on the left. The clonal expansion ability was quantified as fold changes (CUL2 *vs.* Luc). $n=3$. L–N, Western blotting analysis (L), SA-β-Gal staining (M), clonal expansion assay (N), of HGPS hMSCs (P6) following transduction with lentiviruses expressing Luc or CUL2. O, Immunofluorescence analysis of H3K9me3 in RS hMSCs (P8) after transduction with lentiviruses expressing either Luc or CUL2. Representative images were presented on the left. The immunofluorescent intensity was quantified as fold changes (CUL2 *vs.* Luc). The data were analyzed by using two-tailed unpaired Student's *t*-test and are presented as means ±SEM.

https://doi.org/10.1007/s11427-023-2451-3

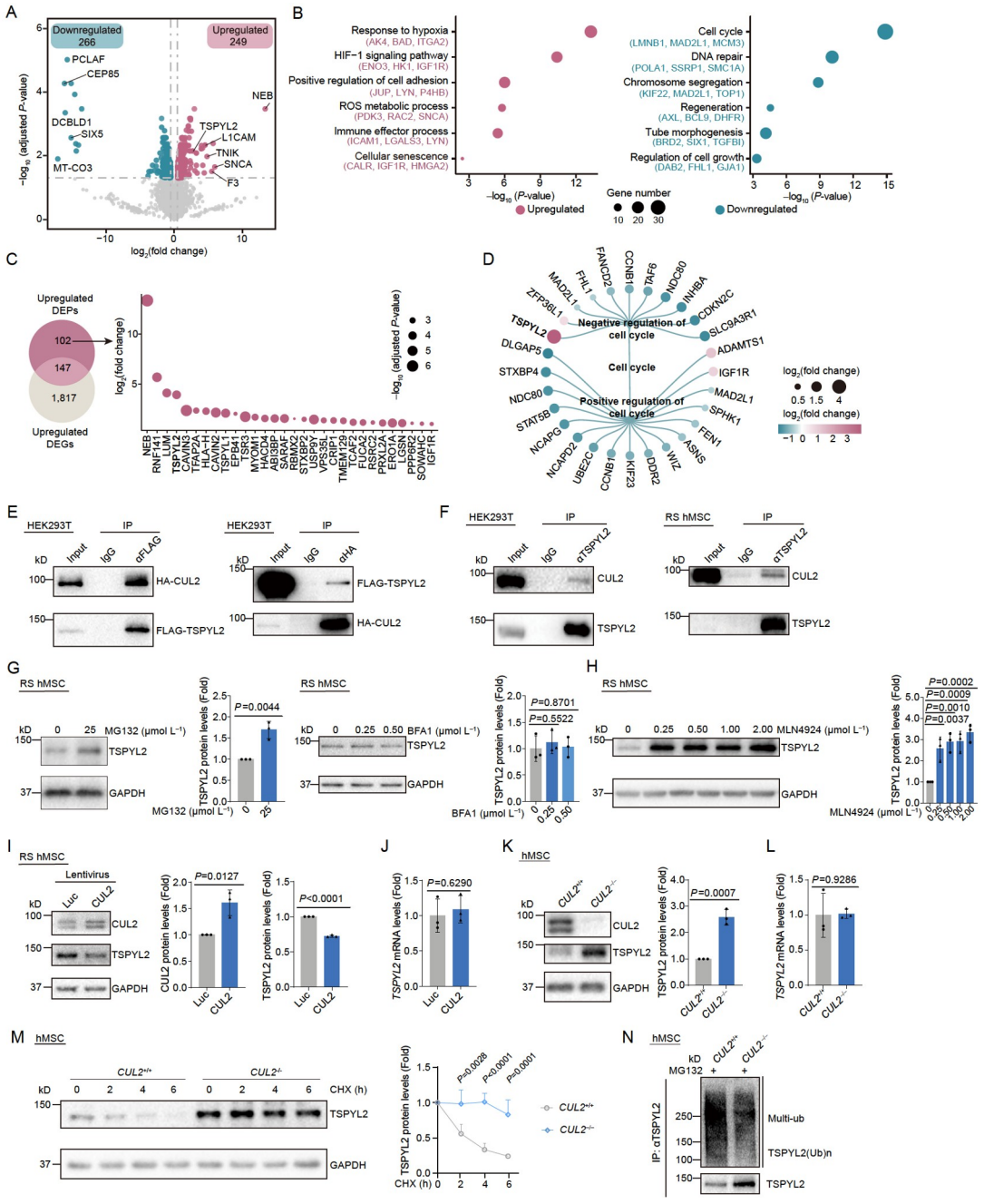

Figure 4. CUL2 degrades TSPYL2 protein through the ubiquitin proteasome pathway. A, Volcano plot visualizing the distribution of DEPs between *CUL2*$^{+/+}$ and *CUL2*$^{-/-}$ hMSCs (P4). B, Point plots displaying GO terms and pathways enriched by upregulated (pink) and downregulated (green) DEPs between *CUL2*$^{+/+}$ and *CUL2*$^{-/-}$ hMSCs (P4). The color keys ranging from grey to pink or to green indicate the degree of enrichment, with lighter shades representing lower enrichment levels and darker shades representing higher enrichment levels. The size of each point corresponds to the number of genes that are enriched in the respective GO term or pathway. Additionally, key DEPs associated with the indicated terms are listed. C, Venn diagram (left) and point plot (right) showing upregulated DEPs without significant changes on transcriptomic level. Point size indicates $-\log_{10}$ (adjusted *P*-value) from low to high. D, Network plot displaying DEPs associated to positive or negative regulation of cell cycle. The color key in the visualization ranges from green to pink represents the $\log_2$(fold change) values of DEPs, from low to high. Node size indicates absolute $\log_2$(fold change). E, HEK293T cells transfected with vectors expressing FLAG-TSPYL2 and HA-CUL2 were harvested for co-immunoprecipitation analysis. IP with anti-FLAG antibody (left), IP with anti-HA antibody (right). F, HEK293T cells and RS hMSCs (P6) were collected for co-immunoprecipitation analysis with anti-TSPYL2 antibody. G, Western blotting showing the expression changes of indicated proteins in RS hMSCs (P6) incubated with MG132 (0 μmol L^{-1}, 5 h), MG132 (25 μmol L^{-1}, 5 h), bafilomycin A1 (0 μmol L^{-1}, 12 h), bafilomycin A1 (0.25 μmol L^{-1}, 12 h) or bafilomycin A1 (0.5 μmol L^{-1},12 h). GAPDH was used as loading control. H, Western blotting showing the expression changes of indicated proteins in RS hMSCs (P6) incubated with different doses of MLN4924 for 24 h. GAPDH was used as loading control. I, Western blotting analysis for the expression levels of the indicated proteins in RS hMSCs (P6) transduced with lentiviruses carrying Luc or CUL2. GAPDH was used as loading control. J, RT-qPCR detection for *TSPYL2* mRNA levels in RS hMSCs (P6) transduced with lentiviruses carrying Luc or CUL2. *GAPDH* was used as loading control. K, Western blotting showing the expression changes of indicated proteins in *CUL2*$^{+/+}$ and *CUL2*$^{-/-}$ hMSCs (P6). GAPDH was used as loading control. L, RT-qPCR detection for *TSPYL2* mRNA levels in *CUL2*$^{+/+}$ and *CUL2*$^{-/-}$ hMSCs (P6). *GAPDH* was used as loading control. M, *CUL2*$^{+/+}$ and *CUL2*$^{-/-}$ hMSCs (P4) were incubated with cycloheximide (CHX, 40 μg mL^{-1}) for the specified durations. Subsequently, Western blotting analysis was conducted using anti-TSPYL2 and GAPDH antibodies. Densitometry analysis was conducted using ImageJ. GAPDH was used as loading control. N, *CUL2*$^{+/+}$ and *CUL2*$^{-/-}$ hMSCs (P6) were exposed to MG132 (25 μmol L^{-1}, 5 h) followed by immunoprecipitation using an anti-TSPYL2 antibody to enrich TSPYL2 proteins. Anti-multi-ubiquitin antibody was used to detect the ubiquitination of TSPYL2. The data were analyzed by using two-tailed unpaired Student's *t*-test and are presented as means±SEM.

tumor growth (Chai et al., 2001; Magni et al., 2019; Tao et al., 2011; Toh et al., 2010), which we found ranked as the top 1 most upregulated protein associated with cell cycle (Figure 4C and D; Figure S3D in Supporting Information). To verify whether TSPYL2 is a potential substrate of CRL2, we co-transfected vectors overexpressing FLAG-TSPYL2 and HA-CUL2 in HEK293T cells, and demonstrated by an interaction between CUL2 and TSPYL2 through co-immunoprecipitation assay (Figure 4E). Moreover, we also found that an endogenous antibody against TSPYL2 could also precipitate CUL2 in HEK293T and WT hMSC (Figure 4F).

Next, we asked whether TSPYL2 protein was degraded through the ubiquitin-proteasome pathway. When we treated WT hMSCs with the proteasome inhibitor MG132, we found an increase in TSPYL2 protein levels, while treatment with the lysosome inhibitor (BFA1) did not change TSPYL2 protein levels (Figure 4G), suggesting that TSPYL2 may be degraded in a ubiquitin-proteasome pathway-dependent manner. We then considered that Cullin neddylation induces conformational changes in CRLs, leading to the activation of CRLs-dependent ubiquitination (Duda et al., 2008; Wang and Liu, 2022). Accordingly, we found that treatment of WT hMSCs with the neddylation inhibitor MLN4924 (Soucy et al., 2009) resulted in a dose-dependent increase of TSPYL2 protein levels (Figure 4H), indicating that TSPYL2 is a potential substrate of CRL E3 ligase. To further confirm that TSPYL2 is regulated by CRL2, we overexpressed CUL2 in hMSCs and found that TSPYL2 protein levels but not mRNA levels decreased (Figure 4I and J). Consistently, we noted elevated TSPYL2 protein levels in *CUL2*$^{-/-}$ hMSCs compared to *CUL2*$^{+/+}$ hMSCs (Figure 4K), a difference that was the result of a prolonged protein half-life without change in its mRNA levels (Figure 4L and M). Next, we asked whether the accumulation of TSPYL2 protein was associated with CRL2-mediated TSPYL2 ubiquitination. As expected, the ubiquitination level of TSPYL2 in *CUL2*$^{-/-}$ hMSCs was much lower than that in *CUL2*$^{+/+}$ hMSCs (Figure 4N). These results collectively support the notion that TSPYL2 acts as a substrate for Cullin E3 ubiquitin ligase complexes (CRLs) and undergoes degradation via the CRL2-mediated ubiquitin-proteasome pathway.

APPBP2 is the substrate receptor of TSPYL2

Since CRLs require substrate receptors to directly degrade their targets (Magni et al., 2019), we would like to identify the CRL2 substrate receptor that can directly target degradation of TSPYL2. When we performed a conjoint analysis of proteins that interact with both CUL2 and TSPYL2 and the known substrate receptor proteins of CRL2 (Figure 5A), we found a potential TSPYL2 substrate receptor protein named APPBP2 (Amyloid Beta Precursor Protein Binding Protein 2) (Figure 5B). Previous studies support that APPBP2 harbors binding degrons (motifs important for regulation of protein degradation rates) for targeting specific substrates (Lin et al., 2018). Accordingly, we identified three potential APPBP2 degrons in the TSPYL2 protein sequence (Figure 5C), further supporting the association between TSPYL2 and APPBP2. In co-immunoprecipitation experiments conducted using HEK293T cells, we co-expressed either FLAG-TSPYL2 and MYC-APPBP2 or FLAG-CUL2 and MYC-APPBP2, and the results showed that TSPYL2 interacts with APPBP2 and that APPBP2 also interacts with CUL2 (Figure 5D and E).

To investigate whether APPBP2 targets TSPYL2 for degradation, we next overexpressed APPBP2 in WT hMSCs and found that TSPYL2 protein levels but not mRNA levels decreased, and that protein levels could be rescued by MG132 treatment (Figure 5F; Figure S3E in Supporting Information). Conversely, we found that silencing APPBP2 using CRISPR/Cas9-mediated knockout and RNA interference led to an increase in TSPYL2 protein levels and an extension of its half-life, while its mRNA levels remained unchanged (Figure 5G–I, Figure S3F and G in Supporting Information). Of note, we found that APPBP2 overexpression promoted the ubiquitination of TSPYL2 *in vivo* (Figure 5J), demonstrating that CRL2^{APPBP2} ubiquitinates TSPYL2 for degradation.

TSPYL2 augments hMSC senescence by promoting p21 expression

Next, we aimed to explore the function of TSPYL2 in hMSC senescence. Firstly, we found that TSPYL2 protein abundance increased in RS hMSCs (Figure 6A). Furthermore, TSPYL2 overexpression was associated with reduced cell proliferation and clonal expansion ability, and accelerated cellular senescence as evidenced by increased SA-β-Gal-positive cells (Figure 6B–E). On the contrary, TSPYL2 knockdown correlated with enhanced cell proliferation, increased clonal expansion ability, and reduced population of senescent cells marked by SA-β-Gal positivity (Figure 6F–I). These findings indicate that TSPYL2 promotes hMSC senescence. To further elucidate whether cellular senescence induced by *CUL2*-deletion was mediated by TSPYL2, we knocked down TSPYL2 in *CUL2*$^{-/-}$ hMSCs, and observed that TSPYL2 knockdown counteracted the reduced cell proliferation and alleviated senescence caused by CUL2 deficiency (Figure 6J–M). Most strikingly, we discovered that TSPYL2 accelerates cellular senescence by promoting P21 expression. Specifically, overexpression of TSPYL2 increased P21 protein levels, whereas knockdown of TSPYL2 downregulated P21 expression (Figure 6N and O). Furthermore, we observed that the reduced clonogenic capacity and increased proportion of senescent cells induced by TSPYL2 overexpression could be partially alleviated by knocking down P21 (Figure 6P and Q; Figure S3H in Supporting Information). Taken together, our findings demonstrate that the CRL2^{APPBP2}-TSPYL2-P21 signaling axis plays a regulatory role against hMSC senescence (Figure 6R).

DISCUSSION

Loss of proteostasis and the exhaustion of stem cells are established hallmarks of aging (Bao et al., 2023; Cai et al., 2012; Cai et al., 2022; Consortium et al., 2023; López-Otín et al., 2023; Pan et al., 2013; Yan et al., 2020). However, our understanding of how human stem cell aging and homeostasis are regulated by CRLs remains limited. In this study, we leveraged multiple senescent hMSC models (RS hMSCs, HGPS hMSCs, and WS hMSCs) to identify CUL2 as a critical Cullin member counteracting hMSC senescence, and found that CRL2^{APPBP2} retarded hMSC senescence by mediating the ubiquitination and degradation of TSPYL2, which further represses P21 expression. These findings help us comprehend the underlying mechanism between protein homeostasis loss and aging and inform development of aging intervention strategies dependent on CRL degradation pathways.

https://doi.org/10.1007/s11427-023-2451-3

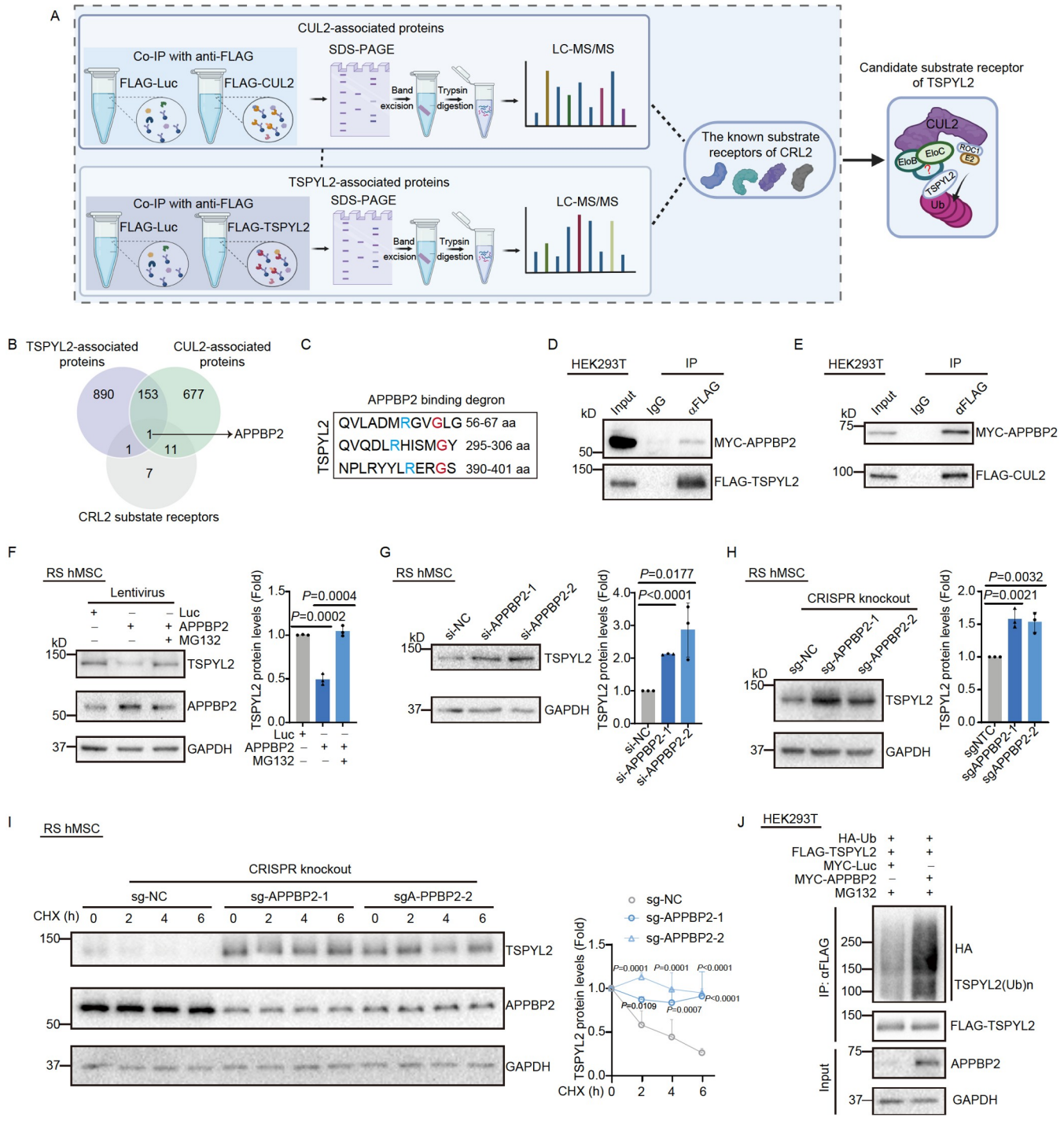

Figure 5. APPBP2 is the substrate receptor of TSPYL2. A, Strategy illustration for identifying substrate receptor proteins of TSPYL2. B, Venn diagram shows the intersection of TSPYL2-associated proteins, CUL2-associated proteins, and known CRL2 substrate receptor proteins. C, The candidate APPBP2 binding degrons of TSPYL2. Critical residues are colored. D, HEK293T cells transfected with vectors expressing FLAG-TSPYL2/MYC-APPBP2 were harvested for co-immunoprecipitation analysis. E, HEK293T cells transfected with vectors expressing FLAG-CUL2/MYC-APPBP2 were harvested for co-immunoprecipitation analysis. F, RS hMSCs (P6) transduced with lentiviruses expressing MYC-Luc, MYC-APPBP2, or MYC-APPBP2 and subsequently incubated with MG132 (25 μmol L^{-1}, 5 h) were subjected to Western blotting analysis for the expression of indicated proteins. GAPDH was used as loading control. G, RS hMSCs (P6) transfected with control siRNA (si-NC), APPBP2 siRNAs (si-APPBP2-1, si-APPBP2-2) were harvested and subjected to Western blotting analysis for TSPYL2 expression. GAPDH was used as loading control. H, Western blotting analysis for TSPYL2 expression in WT hMSCs (P6) transduced with lentiviruses expressing sg-NC or sg-APPBP2. GAPDH was used as loading control. I, RS hMSCs (P6) were transduced with sg-NC or sg-APPBP2 and subsequently incubated with cycloheximide (CHX, 40 μg mL^{-1}) for the indicated times. The cells were then subjected to Western blotting analysis using anti-TSPYL2 and GAPDH antibodies. The relative TSPYL2 protein levels were measured with ImageJ. GAPDH was used as loading control. J, HEK293T cells transduced with specified plasmids were incubated with MG132 (25 μmol L^{-1},5 h). The cells were then lysed for immunoprecipitation assay using anti-FLAG antibody to enrich the FLAG-TSPYL2 proteins. The ubiquitination of FLAG-TSPYL2 was subsequently detected with anti-HA antibody. GAPDH was used as loading control. The data were analyzed by using two-tailed unpaired Student's *t*-test and are presented as means±SEM.

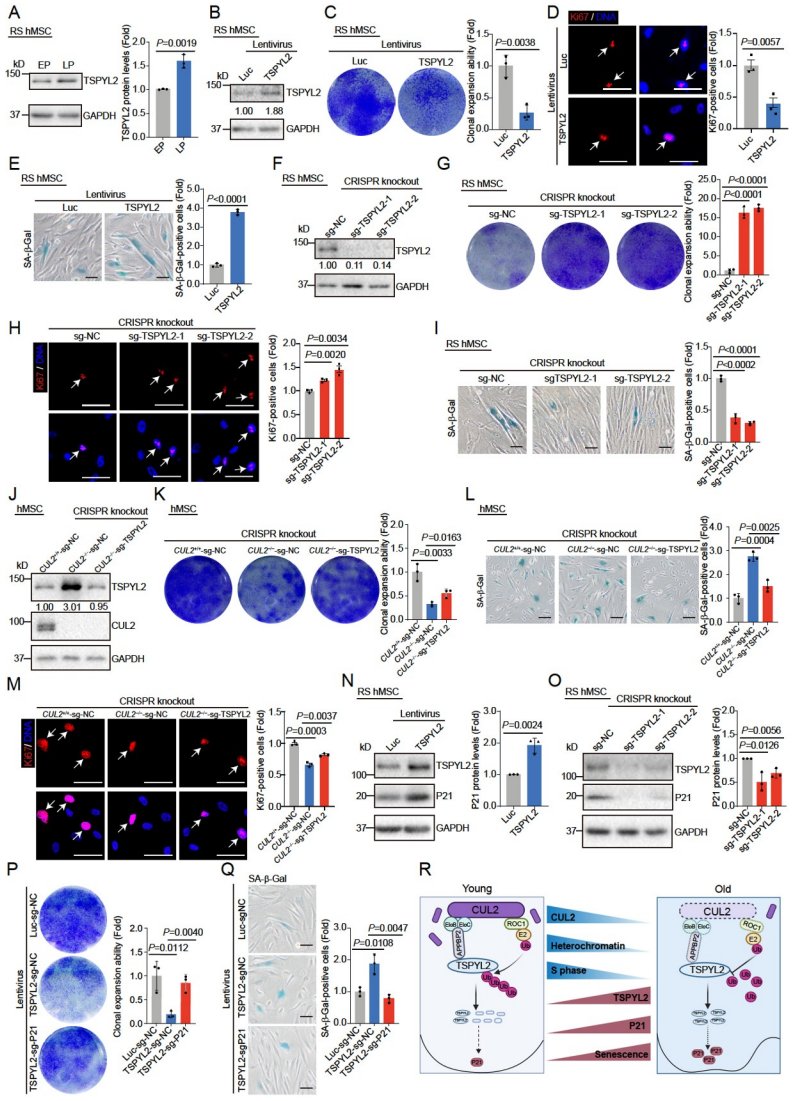

Figure 6. TSPYL2 facilitates hMSC senescence. A, Western blotting analysis for TSPYL2 expression in RS hMSCs. Early passage (EP), P4; late passage (LP), P12. GAPDH was used as loading control. B, Western blotting analysis for TSPYL2 expression in RS hMSCs (P6) that were transduced with lentivirus expressing either Luc or TSPYL2. GAPDH was used as loading control. C, Clonal expansion assay analysis of RS hMSCs (P6) that transduced with lentiviruses expressing either Luc or TSPYL2. Representative images demonstrating the clonal expansion were presented on the left. The clonal expansion ability was quantified as fold changes (TSPYL2 *vs.* Luc). n=3. D, Immunofluorescence analysis of Ki67 in RS hMSCs (P6) that were transduced with lentiviruses expressing either Luc or TSPYL2. Representative images were presented on the left. The proportion of Ki67-positive cells was quantified as fold changes (TSPYL2 *vs.* Luc). n=3. Scale bars, 50 μm. E, SA-β-Gal staining was performed on RS hMSCs (P6) that were transduced with lentiviruses expressing either Luc or TSPYL2. Representative images were presented on the left. The proportion of SA-β-Gal-positive cells was quantified as fold changes (TSPYL2 *vs.* Luc). n=3. Scale bars, 100 μm. F, Western blotting analysis of TSPYL2 expression in RS hMSCs (P6) transduced with lentiviruses expressing sg-NC or sg-TSPYL2. GAPDH was used as loading control. G, Clonal expansion assay was performed on RS hMSCs (P6) that were transduced with lentiviruses expressing either sg-NC or sg-TSPYL2. Representative images were presented on the left. The clonal expansion ability was quantified as fold changes (sg-TSPYL2 *vs.* sg-NC). n=3. H, Immunofluorescence analysis of Ki67 in RS hMSCs (P6) that were transduced with lentiviruses expressing either sg-NC or sg-TSPYL2. Representative images were presented on the left. The proportion of Ki67-positive cells was quantified as fold changes (sg-TSPYL2 *vs.* sg-NC). n=3. Scale bars, 50 μm. I, SA-β-Gal staining was performed on RS hMSCs (P6) following transduction with lentiviruses expressing either sg-NC or sg-TSPYL2. Representative images were showed on the left. The proportion of SA-β-Gal-positive cells was quantified as fold changes (sg-TSPYL2 *vs.* sg-NC). n=3. Scale bars, 100 μm. J, Western blotting showing the expression changes of indicated proteins in $CUL2^{+/+}$ hMSCs, $CUL2^{-/-}$ hMSCs (P6) infected with lentivirus expressing sg-NC or sg-TSPYL2. GAPDH was used as loading control. K, Clonal expansion assay was performed on $CUL2^{+/+}$ or $CUL2^{-/-}$ hMSCs (P6) transduced with lentivirus expressing sg-NC or sg-TSPYL2. Representative images were presented on the left. The clonal expansion ability was quantified as fold changes ($CUL2^{-/-}$-sg-NC *vs.* $CUL2^{+/+}$-sg-NC, $CUL2^{-/-}$-sg-TSPYL2 *vs.* $CUL2^{-/-}$-sg-NC). n=3. L, SA-β-Gal staining was performed on $CUL2^{+/+}$, or $CUL2^{-/-}$ hMSCs (P6) transduced with lentivirus expressing either sg-NC or sg-TSPYL2. Representative images were presented on the left. The proportion of SA-β-Gal-positive cells was quantified as fold changes ($CUL2^{-/-}$-sg-NC *vs.* $CUL2^{+/+}$-sg-NC, $CUL2^{-/-}$-sg-TSPYL2 *vs.* $CUL2^{-/-}$-sg-NC). n=3. Scale bars, 100 μm. M, Immunofluorescence analysis of Ki67 in $CUL2^{+/+}$ or $CUL2^{-/-}$ hMSCs (P6) transduced with lentivirus expressing either sg-NC or sg-TSPYL2. Representative images were presented on the left. The proportion of Ki67-positive cells was quantified as fold changes ($CUL2^{-/-}$-sg-NC *vs.* $CUL2^{+/+}$-sg-NC, $CUL2^{-/-}$-sg-TSPYL2 *vs.* $CUL2^{-/-}$-sg-NC). n=3. Scale bars, 100 μm. N, Western blotting showing the expression changes of indicated proteins in RS hMSCs (P6) following transduction with lentiviruses expressing either Luc or TSPYL2. GAPDH was used as loading control. O, Western blotting showing the expression changes of indicated proteins in RS hMSCs (P6) transduced with lentivirus expressing sgNC or sgTSPYL2. GAPDH was used as loading control. P, Clonal expansion assay was performed on RS hMSCs transduced with lentivirus expressing Luc-sg-NC, TSPYL2-sg-NC, or TSPYL2-sg-P21. Representative images were presented on the left. Clonal expansion ability is quantified as fold changes (TSPYL2-sg-NC *vs.* Luc-sg-NC, TSPYL2-sg-P21 *vs.* Luc-sg-NC). n=3. Q, SA-β-Gal staining analysis on RS hMSCs (P4) transduced with lentivirus expressing Luc-sg-NC, TSPYL2-sg-NC, or TSPYL2-sg-P21. Representative images were showed on the left. The proportion of SA-β-Gal-positive cells was quantified as fold changes (TSPYL2-sg-NC *vs.* Luc-sg-NC, TSPYL2-sg-P21 *vs.* Luc-sg-NC). n=3. Scale bars, 100 μm. R, A working model of $CRL2^{APPBP2}$-mediated ubiquitination of TSPYL2 to regulate hMSC senescence. The data were analyzed by using two-tailed unpaired Student's *t*-test and are presented as means±SEM.

https://doi.org/10.1007/s11427-023-2451-3

CRLs, as the most extensive multi-subunit E3 ubiquitin ligase family, govern various biological events such as the cell cycle, transcription, and cell growth, by controlling the degradation of varied substrate proteins (Petroski and Deshaies, 2005; Sarikas et al., 2011). Although some studies support a general association between CRLs and aging, there is, to our knowledge, a paucity of knowledge about whether specific Cullin proteins directly regulate cellular senescence. In this study, we examined the impact of various Cullin family members in three distinct human senescent stem cell models with divergent genetic backgrounds. Our observations revealed that CUL1 knockdown promoted senescence exclusively in RS hMSCs, while depletion accelerated senescence solely in HGPS hMSCs. Remarkably, the knockdown of CUL2 emerged as the common trigger for cellular senescence across all three models. Consequently, we elected to center our focus on CUL2 in this study. Supplementing our findings, previous investigations have underscored the role of Cullin protein neddylation inhibitor MLN4924 in inducing cellular senescence (Jia et al., 2011; Lin et al., 2010). Additionally, multiple CRLs have been implicated in the regulation of cellular senescence and worm lifespan (Chen et al., 2018; Choppara et al., 2018; Johmura et al., 2020; Li and Xiong, 2017; Xu et al., 2008).

It is noteworthy that distinct members within the Cullin protein family might exert their influence through modulation of distinct substrates in the context of cellular senescence. For example, the substrate receptors of CUL1, namely FBXO22 and FBXO31, were found to delay cellular senescence through the ubiquitination and degradation of their substrates P53 and FBXO31, respectively (Choppara et al., 2018; Johmura et al., 2020). CUL7 was found to regulate cellular senescence through the targeted degradation of IRS1 (Xu et al., 2008). Here, we uncovered that CUL2 depletion led to impaired degradation of TSPYL2, eventually contributing to increased P21 expression. Our results together with existing literature suggest that Cullin family members may differentially regulate cellular senescence, which is potentially influenced by the genetic background and the distinct substrates they target.

Complementing previous studies showing that CUL2 primarily forms functional E3 ligase complexes with EloB/EloC and substrate receptor proteins to ubiquitinate and degrade substrates (Petroski and Deshaies, 2005; Zimmerman et al., 2010), we here identified TSPYL2 as a specific CRL2 substrate and discovered that its overexpression promotes hMSC senescence by upregulating P21. In support of this mechanism, TSPYL2 has been linked to multiple biological processes, comprising prevention of proliferation, and inhibition of the cell cycle (Magni et al., 2019; Tao et al., 2011; Toh et al., 2010; Tu et al., 2011). In this study, we discovered the significant involvement of TSPYL2 in modulating hMSC homeostasis and proposed that TSPYL2 acts as a senescence-promoting factor, adding a direct link between TSPYL2 and cellular senescence. Nevertheless, the relationship between TSPYL2 and organismal aging warrants further investigation.

Further, we demonstrated that TSPYL2 facilitated cellular senescence by augmenting P21 expression, and observed an accumulation of DNA damage upon CUL2 deficiency. In fact, one study has established the link between TSPYL2-mediated upregulation of P21 and DNA damage (Tao et al., 2011). Specifically, TSPYL2 can induce the accumulation of P53 protein, thereby upregulating P21 expression in mouse embryonic fibroblasts (MEFs) under DNA damage stimulation, but hardly affecting DNA damage repair (Tao et al., 2011). Furthermore, through the investigation of CUL2's interactome and quantitative proteomic analysis, we have uncovered that CUL2 may potentially elevate the levels of P21 by modulating various DNA damage repair proteins, including but not limited to SETD2 (SET domain-containing protein 2), UBQLN4 (Ubiquilin 4), MGMT (O6-methylguanine-DNA methyl-transferase) through different mechanism. These pieces of evidence together with ours suggest that the upregulation of P21 by TSPYL2 in CUL2-deficient hMSCs may involve DNA damage repair mechanism. Additionally, TSPYL2 may augment P21 expression by other mechanisms. First, it has been reported that TSPYL2 regulates P21 expression in a P53-dependent mechanisms in HeLa cells. On one hand, it disrupts MDM2-mediated protein degradation of P53, leading to increased P53 levels. On the other hand, it activates the MEK/ERK1/2 MAPK signaling pathway, which enhances the binding of P53 to *CDKN1A* (*P21*) promoter region, thereby upregulating P21 expression (Tu et al., 2007). Second, given its role as a nucleosome assembly protein, TSPYL2 interacts with transcriptional complexes and enables chromatin remodeling to modulate gene expression. For instance, TSPYL2 serves as an essential component of the REST/NREF complex involved in TGF-β signaling activation (Epping et al., 2015), can be recruited to the promoters of specific EZH2 target genes in neurons, and promotes their expression to facilitate normal neuronal maturation and function (Liu et al., 2019), and regulates the expression of GluN2A and GluN2B by binding to CBP to modulate cognitive variability in mice (Tsang et al., 2014). Consequently, it is plausible that TSPYL2 may regulate P21 expression by interacting with other transcriptional complexes. Third, TSPYL2 has been found to disrupt the interaction between SIRT1 and its downstream targets, leading to increased acetylation levels of P53 and P53-dependent cell death in U2OS cells (Magni et al., 2019). Overall, TSPYL2 likely modulates P21 expression through multiple pathways, necessitating further experimental investigations to ascertain its precise regulatory mechanisms in our human mesenchymal stem cell system.

In a fully functional Cullin-2 based E3 ubiquitin ligase, substrate receptor proteins directly bind to substrates, determining substrate specificity (Sarikas et al., 2011; Zimmerman et al., 2010). Currently, around 20 known substrate receptor proteins have been reported to regulate various biological processes, including tumor development, germ cell differentiation, and viral defense by degrading specific substrates (Cai and Yang, 2016; Okumura et al., 2012). In this study, we identified that APPBP2 directly recognizes TSPYL2 as its substrate receptor for subsequent ubiquitination and degradation. In support of this mechanism, a recent study revealed that APPBP2 acts as a substrate protein receptor for PRDM16 (PR/SET domain 16), degrading PRDM16 and thereby controlling the biogenesis of beige fat (Wang et al., 2022a). Our study deepens the understanding of the functional APPBP2 paradigm.

In summary, this study elucidates an unappreciated function of CUL2 in safeguarding hMSC aging and uncovers the molecular mechanism through which $CRL2^{APPBP2}$ counteracts hMSC senescence via ubiquitin-mediated degradation of TSPYL2. Our findings add a new layer to our understanding of the relationship between loss of proteostasis and aging, and suggest potential new targets for development of intervention against aging and age-associated disorders.

MATERIALS AND METHODS

Animal experiments

All animal experiments in this study followed the guidelines for animal work and were approved from the Xuanwu Hospital, Capital Medical University Animal Care and Use Committee. All the male NOD/SCID mice (4 weeks old) were purchased from SPF (Beijing) Biotechnology.

To generate teratoma, 4×10^6 *CUL2*$^{+/+}$ or *CUL2*$^{-/-}$ hESCs in a mixture of Matrigel (BD Biosciences, USA) and mTeSR medium (STEMCELL Technologies, USA) at a 1:4 ratio were subcutaneously injected into NOD/SCID mice. The implanted mice were monitored for approximately 8 weeks, and the collected teratomas were subjected to further analysis. The hMSC implantation assay followed a previously described protocol (Zhao et al., 2022). Briefly, 1×10^6 *CUL2*$^{+/+}$ or *CUL2*$^{-/-}$ hMSCs (P5) transduced with lentivirus expressing luciferase were injected into the tibialis anterior muscles of male nude mice (6 weeks old). The luciferase signals were captured at 0, 1, 2, 3, and 4 d post-injection using the Xenogen In Vivo Imaging System (IVIS) Spectrum (Xenogen; Caliper, PerkinElmer, USA).

Cell culture

To establish a cell model for investigating the function of the *CUL2* gene, we generated *CUL2*$^{-/-}$ hESCs by deleting the *CUL2* gene in H9 hESCs (WiCell Research Institute, USA). Both *CUL2*$^{+/+}$ and *CUL2*$^{-/-}$ hESCs were cultured on mitomycin C-inactivated MEF feeder layers using hESC culture medium. The hESC culture medium consists of DMEM/F-12 (Thermo Fisher Scientific, USA) supplemented with 20% knockout serum replacement (Thermo Fisher Scientific), 2 mmol L^{-1} GlutaMAX (Thermo Fisher Scientific), 0.1 mmol L^{-1} Non-Essential Amino Acids (NEAA, Thermo Fisher Scientific), 1% Penicillin-Streptomycin (PS, Thermo Fisher Scientific), 55 μmol L^{-1} β-mercaptoethanol (Sigma-Aldrich, USA), and 10 ng mL^{-1} bFGF (Joint Protein Central, Republic of Korea). Alternatively, hESCs can be cultured on Matrigel-coated plates using mTeSR medium. hMSCs were cultured in hMSC culture medium, which consists of MEMα basal medium (Thermo Fisher Scientific) supplemented with 10% fetal bovine serum (FBS, Gibco, USA), 1% PS, 0.1 mmol L^{-1} NEAA, and 1 ng mL^{-1} bFGF. HEK293T cells were cultured in DMEM/High glucose (Cytiva, USA) supplemented with 10% FBS and 1% PS.

Generation of *CUL2*$^{-/-}$ hESCs

Knockout of *CUL2* was accomplished by utilizing the CRISPR/Cas9 system as previously described (He et al., 2023; Li et al., 2023; Pan et al., 2016; Wang et al., 2023; Zhang et al., 2022a; Zhao et al., 2022). In brief, the pCAG-mCherry-gRNA vector (Addgene, #87110) was employed to clone sgRNAs that targeted exon 3 of the *CUL2* gene. Prior to gene knockout, wildtype (WT) hESCs were cultured in mTeSR medium supplemented with Y-27632, a ROCK inhibitor (Selleck, USA), for a duration of 24 h. Electroporation of the indicated vectors was performed on WT hESCs with a 4D Nucleofector (Lonza, Switzerland). After electroporation, the cells were maintained on Matrigel-coated plates with mTeSR medium containing Y-27632 for an additional 48 h. Fluorescence-activated cell sorting (FACS) system was used to sort GFP and mCherry double-positive cells. Subsequently, these sorted cells were cultured on MEF feeders using the hESC culture medium. The candidate hESCs were collected for genomic DNA sequencing and Western blotting analysis. For the sgRNA sequences targeting *CUL2* and primers used in this study, please refer to Table S1 in Supporting Information.

Directed differentiation and characterization of *CUL2*$^{+/+}$ and *CUL2*$^{-/-}$ hMSCs

CUL2$^{+/+}$ or *CUL2*$^{-/-}$ hMSCs were generated from *CUL2*$^{+/+}$ or *CUL2*$^{-/-}$ hESCs following the protocols as previously described (Bi et al., 2020; Lei et al., 2023; Liang et al., 2021). Briefly, *CUL2*$^{+/+}$ or *CUL2*$^{-/-}$ hESCs were cultured on MEF feeders, then digested with dispase, and seeded on low-adhesion plate for 72 h to generate embryoid bodies (EBs). These EBs were then transferred onto Matrigel-coated 6-well plates to initiate differentiation using hMSC differentiation medium. The hMSC differentiation medium comprises of MEMα basal medium supplemented with 10% FBS, 0.1 mmol L^{-1} NEAA, 5 ng mL^{-1} TGFβ (HumanZyme, USA), 1 ng mL^{-1} bFGF, and 1% PS. After approximately 10 d, the cells were transferred and maintained in hMSC culture medium. Upon reaching 90% confluence, the positive markers (CD105, CD73, and CD90) were used to purify hMSCs by employing a FACS system (BD FACS Calibur). Furthermore, the negative markers (CD14, CD19, and CD34) were used to validate the purity of the hMSC by flow cytometry.

The following antibodies used for FACS assay were listed as follows: anti-CD73-PE (BD Biosciences, 1:200), anti-CD90-FITC (BD Biosciences, 1:300), anti-CD105-APC (BD Biosciences, 1:200), anti-CD14-PE (BD Biosciences, 1:200), anti-CD19-APC (BD Biosciences, 1:200), and anti-CD34-FITC (BD Biosciences, 1:200).

The differentiation potential of *CUL2*$^{+/+}$ or *CUL2*$^{-/-}$ hMSCs into adipocytes, osteoblasts, and chondrocytes was assessed by Oil Red O (adipogenesis), Von Kossa (osteogenesis), and Toluidine Blue (chondrogenesis) staining, respectively.

Clonal expansion assay

The clonal expansion assay was conducted according to a previously reported study (Zhang et al., 2023). Briefly, cells were dissociated into single cells using TrypLE^{TM} express enzyme. 2,000 cells were subsequently seeded in each well of 12-well plates. Following a culture period of approximately 12 d, the cells were washed twice with PBS, fixed in a 4% paraformaldehyde (PFA) solution for a duration of 30 min, and subsequently stained with crystal violet solution (Biohao, Wuhan, China). The images were captured with the Epson Perfection V370 Photo scanner. The relative colony density was quantified with ImageJ software as previously described (Ren et al., 2019).

SA-β-Gal staining

SA-β-Gal staining of hMSCs was performed as described previously (Geng et al., 2023; Huang et al., 2022; Kubben et al., 2016; Liu et al., 2023; Zhu et al., 2022). First, the hMSCs were washed twice with PBS. Next, the cells were subjected to a fixing buffer (2% formaldehyde, 0.2% glutaraldehyde in PBS) for a duration of 5 min. Next, the cells were stained in SA-β-Gal

https://doi.org/10.1007/s11427-023-2451-3

staining buffer (composed of 5 mmol L^{-1} $K_4[Fe(CN)_6]$, 5 mmol L^{-1} $K_3[Fe(CN)_6]$, 150 mmol L^{-1} NaCl, 40 mmol L^{-1} citric acid/Na phosphate buffer pH6.0, 2 mmol L^{-1} $MgCl_2$, and 1 mg mL^{-1} X-Gal) at 37°C overnight. The resulting stained cells were then imaged using a digital microscope camera (Olympus, Japan) and quantified with ImageJ 1.37v software.

Cell cycle phase analysis

Cell cycle phase analysis was conducted following a previously established protocol (Fu et al., 2019). Briefly, cells were harvested and subjected to flow cytometer after propidium iodide (PI) staining. 10,000 cells were collected and subjected to cycle analysis using ModFit software.

Flow cytometry analysis of cell apoptosis and cellular ROS

Measurement of cell apoptosis was performed following the instruction of the Annexin V-EGFP Apoptosis Detection Kit (Vigorous Biotechnology, Beijing, China) for both *CUL2*$^{+/+}$ and *CUL2*$^{-/-}$ hMSCs. Cellular ROS levels were assessed in *CUL2*$^{+/+}$ or *CUL2*$^{-/-}$ hMSCs using H2DCFDA probe (Thermo Fisher Scientific). The apoptotic cells and cellular ROS were quantified by FACS.

Immunofluorescence staining

To perform immunofluorescence staining, cells were seeded on coverslips (Thermo Fisher Scientific) and subjected to immunofluorescence staining at 80% confluence. Following the washes with PBS, the cells were fixed with 4% PFA and subsequently permeabilized with 0.4% Triton X-100. Next, the cells were subjected to blocking with 10% donkey serum (Jackson ImmunoResearch, USA) for a duration of 1 h at room temperature. The cells were incubated with primary antibodies overnight at 4°C, followed by an incubation with secondary antibodies. The cells were finally mounted using Vector Labs mounting medium, and confocal images were captured using Zeiss-LSM900 imaging system.

The antibodies utilized for immunofluorescence staining were listed below: anti-OCT4 (Santa Cruz, USA, 1:200), anti-SOX2 (R&D, USA, 1:200), anti-NANOG (Abcam, UK, 1:200), anti-Ki67 (ZSGB-BIO, Beijing, China, 1:1,000), anti-H3K9me3 (Abcam, 1:1,000), anti-LAP2β (BD Biosciences, 1:1,000), anti-TuJ1 (Sigma-Aldrich, 1:500), anti-SMA (Sigma-Aldrich, 1:500), anti-FOXA2 (Cell Signaling Technology, USA, 1:500), anti-Lamin B1 (Abcam, 1:500), anti-HP1α (Cell Signaling Technology, 1:500), anti-γH2AX (Millipore, USA, 1:1,000), Alexa 488 donkey anti-mouse IgG (Thermo Fisher Scientific, 1:500), and Alexa 568 donkey anti-rabbit IgG (Thermo Fisher Scientific, 1:500). Nuclear DNA staining was performed using Hoechst 33342 (Thermo Fisher Scientific).

Cycloheximide chase assay

For protein half-life analysis, cells were incubated with cycloheximide (CHX, Sigma-Aldrich) for 0, 2, 4, or 6 h. Subsequently, the cells were collected, lysed, and subjected to Western blotting analysis. The relative TSPYL2 protein intensities were quantified using ImageJ 1.37v software.

RT-qPCR

RNA isolation from hMSCs was performed using TRIzol reagent (Thermo Fisher Scientific). The cDNAs were synthesized using HiScript II Q Select RT SuperMix for qPCR (+gDNA wiper) (Vazyme, Nanjing, China). Quantitative real-time PCR was performed using NovoStart®SYBR qPCR SuperMix Plus (Novoprotein, Suzhou, China) on the Bio-Rad CFX Opus 384 Real-Time PCR System. The quantitative reverse transcription PCR (RT-qPCR) primers used are listed in Table S1 in Supporting Information.

Plasmid construction

cDNA derived from hMSCs was employed for amplification of the full-length target genes. The sequence information for human *CUL2* (NM_001198777.2), *TSPYL2* (NM_022117.4), and *APPBP2* (NM_006380.5) was acquired from the National Center for Biotechnology Information (NCBI). Human Flag-tagged CUL2, Flag-tagged TSPYL2 and HA-tagged CUL2 were cloned into the pLE4 vector (a gift from Tomoaki Hishida) (Deng et al., 2019), respectively, with pLE4-Luc (Luciferase) as a control. Human MYC-tagged APPBP2 and MYC-tagged CUL2 were cloned into the pHBLV-CMVIE-IRES-puro (pHBLV) vector (kindly provided by Dr. Tanjun Tong). Lentiviral CRISPR/Cas9-mediated knockout experiments were performed by cloning sgRNAs targeting each member of the Cullin family, *TSPYL2*, *APPBP2*, or *CDKN1A* (*P21*) into the lenti-CRISPRv2 vector (Addgene, #52961). Lentiviral CRISPR/Cas9-mediated activation involved cloning the sgRNA of CUL2 into the lentiSAMv2 vector (Addgene, #75112). Lentiviral shRNA-mediated knockdown employed the cloning of the *CUL2* shRNA into the pLVTHM vector (Addgene, #12247).

All primers utilized for plasmid construction are listed in Table S1 in Supporting Information.

Co-immunoprecipitation (Co-IP)

Cells were harvested and subjected to lysis on ice using a lysis buffer containing 50 mmol L^{-1} Tris-HCl (pH 7.4), 150 mmol L^{-1} NaCl, 0.3% NP-40, 1 mmol L^{-1} EDTA, 1 mmol L^{-1} PMSF, and 1× cocktail. For immunoprecipitation (IP), the protein extract was subjected to an overnight incubation at 4°C with continuous rotation in the presence of specific antibodies (2 μg). Subsequently, the protein extracts were further incubated with Protein A/G plus agarose beads (Santa Cruz) for 3 h with constant rotation. After thorough washing, the precipitated proteins were subjected to analysis using Western blotting. The antibodies employed for immunoprecipitation and Western blotting included: anti-FLAG (Sigma-Aldrich), anti-MYC-tag (MBL, Japan), anti-TSPYL2 (Proteintech, Wuhan, China), anti-CUL2 (Santa Cruz), normal rabbit IgG control (Cell Signaling Technology), and mouse IgG control (Cell Signaling Technology).

Western blotting

hESCs or hMSCs were subjected to lysis using RIPA lysis buffer supplemented with cocktail (Roche, USA) for 30 min on ice. The protein extracts were quantified using the BCA Protein Assay Kit (Dingguo Changsheng, Beijing, China) and separated by SDS-PAGE. Antibodies used for Western blot analysis included: anti-

CUL2 (Santa Cruz, 1:2,000), anti-TSPYL2 (Proteintech, 1:2,000), anti-LAP2β (BD Biosciences, 1:1,000), anti-HP1α (Cell Signaling Technology, 1:2,000), anti-Lamin B1 (Abcam, 1:1,000), anti-P21$^{waf/cip1}$ (Cell Signaling Technology, 1:1,000), anti-APPBP2 (Abclonal, USA, 1:1,000), anti-β-Tubulin (Immunoway, USA, 1:3,000), anti-GAPDH (Santa Cruz, 1:4,000), goat anti-Mouse IgG (ZSGB-bio, 1:5,000), and goat anti-Rabbit IgG (ZSGB-bio, 1:5,000).

In vivo ubiquitination assay

To perform *in vivo* ubiquitination assay, HEK293T cells transfected with various combinations of FLAG-TSPYL2, HA-ubiquitin (HA-Ub), and MYC-Luc, MYC-APPBP2, or MYC-CUL2 were incubated with MG132 (Selleck, Shanghai, China, 25 μmol L^{-1}) for 5 h before lysate collection and immunoprecipitation analysis. Ubiquitylated proteins were detected with anti-FLAG (Sigma-Aldrich), anti-MYC-tag (MBL) or anti-HA-tag (Cell Signaling Technology) antibodies. In addition, *CUL2*$^{+/+}$ hMSCs and *CUL2*$^{-/-}$ hMSCs (P6) incubated with MG132 (25 μmol L^{-1}) for 5 h were subjected to immunoprecipitation analysis with anti-TSPYL2 (Proteintech). Anti-multi-ubiquitin (MBL 1:3,000) and anti-TSPYL2 (Proteintech, 1:2,000) were used to detect ubiquitylated TSPYL2 proteins.

RNA-seq data processing

To process the RNA-seq raw data, we first eliminated low-quality reads and adaptor-containing sequences using Trim Galore (version 0.4.5). The resulting trimmed data were then aligned to the human hg19 reference genome using STAR (version 2.7.1a) software with strand-specific parameters (Dobin et al., 2013). Gene expression levels were determined by counting the reads assigned to each gene using featureCounts (version 2.0.1) (Liao et al., 2014). To identify differentially expressed genes (DEGs), we used a criterion of absolute $\log_2$(fold change) over 0.5 and Benjamini-Hochberg adjusted *P*-value less than 0.05, as implemented in the R package DESeq2 (version 1.38.1) (Love et al., 2014). We used Metascape (Zhou et al., 2019) to identify enriched GO terms and pathways. The DEGs are listed in Table S2 in Supporting Information.

Coomassie blue staining and LC-MS/MS

HEK293T cells expressing FLAG-tagged-Luc, FLAG-tagged CUL2, or FLAG-tagged TSPYL2 were harvested and lysed using immunoprecipitation lysis buffer (50 mmol L^{-1} Tris-HCl, pH 7.4, 150 mmol L^{-1} NaCl, 0.3% NP-40, 1 mmol L^{-1} EDTA, 1 mmol L^{-1} PMSF) containing protease inhibitor cocktail (Roche). The lysate was incubated overnight at 4°C with anti-FLAG M2 Affinity Gel (Sigma-Aldrich). After several extensive washes, the enriched protein complexes were eluted using excess FLAG peptide. The eluted proteins were separated by SDS-PAGE and visualized by Coomassie blue (Dingguo Changsheng) staining. The protein bands of interest were excised and subjected to liquid chromatography-tandem mass spectrometry (LC-MS/MS) analysis with Q Exactive mass spectrometer (Thermo Fisher Scientific). The interacting proteins of CUL2 or TSPYL2 are listed in Tables S3 and S4 in Supporting Information.

DIA quantitative proteomics

Data-independent acquisition (DIA) quantitative proteomic was performed by Beijing Proteome Research Center. Briefly, 1×10^7 *CUL2*$^{+/+}$ and *CUL2*$^{-/-}$ hMSCs were lysed in lysis buffer (8 mol L^{-1} UREA, 100 mmol L^{-1} Tris-HCl, pH 7.6, with protease inhibitors) on ice for 30 min. After centrifuging at 18,000×*g* for 15 min, the supernatant was collected and the protein concentration was quantified using the BCA assay (Dingguo Changsheng), Beijing, China and applied the filter-aided sample preparation (FASP) enzymatic digestion method to digest 6 samples (Wiśniewski et al., 2009). Each sample is subjected to enzymatic digestion with 2 μg of peptides. Mass spectrometry analysis was conducted using Thermo Q Exactive HF mass spectrometer (Thermo Fisher Scientific) for a single 120-min DIA experiment. The mass spectrometric data were processed by Spectronout Pulsar 16.1 (Biognosys) using the DirectlyDIA method (Wang et al., 2022b).

Peptide identification was performed by searching against the UniProt human database. *P*-value was calculated using the kernel density estimator, and *Q*-value cutoff at precursor and protein levels were set to 0.01. Protein abundances were quantified by the peak area of production, with at least three product ions selected for average intensity quantification. The protein abundances were $\log_2$-transformed and normalized by column-wise median centering. Determination of differentially expressed proteins (DEPs) was carried out using the R package limma (version 3.50.3). DEPs were defined as those with a Benjamini-Hochberg adjusted *P*-value of less than 0.05 and absolute $\log_2$(fold change) greater than 0.485. The DEPs information is listed in Table S5 in Supporting Information.

CNV analysis

Whole-genome sequencing was conducted following established protocols (Pan et al., 2016; Yan et al., 2019). In brief, genomic DNAs were extracted using the DNeasy Blood & Tissue Kit (QIAGEN, Germany) and subjected to DNA quality control, library construction and sequencing. The initial step of bioinformatic analysis included trimming the raw reads using Trim Galore (version 0.4.5), followed by alignment to the human hg19 genome using Bowtie2 (version 2.2.9) (Langmead and Salzberg, 2012). Subsequently, read counts were obtained for each 500-kb bin using the "readCounter" function from the hmmcopy_utils tool (https://github.com/shahcompbio/hmmcopy). To correct for GC content, copy number, and mappability effects, we employed the R/Bioconductor package HMMcopy (version 1.26.0).

Statistical analysis

Two-tailed unpaired Student's *t*-test was conducted using GraphPad Prism 8 Software. The data were presented as means ±SEM. Statistical significance was defined as a *P*-value less than 0.05. For DEG analysis, the Wald test was applied using R package DESeq2 (version 1.38.1). *P*-value for DEGs and DEPs were adjusted by Benjamini-Hochberg procedure.

Data availability

The transcriptomic and whole genome sequencing data generated in this study have been deposited in the Genome Sequence Archive (Chen et al., 2021) at the National Genomics Data

Center, China National Center for Bioinformation, Chinese Academy of Sciences, with accession number HRA004808. The proteomic data obtained in this study have been deposited in the iProX partner repository (Chen et al., 2022) and are available through the ProteomeXchange Consortium (http://proteome-central.proteomexchange.org) under the accession numbers PXD042924 and PXD043036. The differentially expressed genes identified in *CUL2*$^{-/-}$ hMSCs have been submitted and deposited in the Aging Atlas (AA, https://ngdc.cncb.ac.cn/aging/index) databases (Atlas, 2021).

Compliance and ethics

The author(s) declare that they have no conflict of interest.

Acknowledgement

This work was supported by the National Key Research and Development Program of China (2020YFA0804000, 2022YFA1103700, 2020YFA0112200, 2021YFF1201000, the STI2030-Major Projects-2021ZD0202400, 2022YFA1103800), the National Natural Science Foundation of China (82201714, 81921006, 82125011, 92149301, 92168201, 91949209, 92049304, 92049116, 32121001, 82192863, 82122024, 82071588, 32000500, 82271600, 82001477, 82201727), the Strategic Priority Research Program of the Chinese Academy of Sciences (XDA16000000), CAS Project for Young Scientists in Basic Research (YSBR-076, YSBR-012), the Program of the Beijing Natural Science Foundation (Z190019), the Fellowship of China Postdoctoral Science Foundation (2022M712216), the Project for Technology Development of Beijing-affiliated Medical Research Institutes (11000023T000002036310), the Pilot Project for Public Welfare Development and Reform of Beijing-affiliated Medical Research Institutes (11000022T000000461062), Youth Innovation Promotion Association of CAS (E1CAZW0401, 2022083, 2023092), Young Elite Scientists Sponsorship Program by CAST (YESS20200012, YESS20210002), the Informatization Plan of Chinese Academy of Sciences (CAS-WX2021SF-0301, CAS-WX2022SDC-XK14, CAS-WX2021SF-0101), New Cornerstone Science Foundation through the XPLORER PRIZE (2021-1045), Excellent Young Talents Program of Capital Medical University (12300927), Excellent Young Talents Training Program for the Construction of Beijing Municipal University Teacher Team (BPHR202203105), and Beijing Hospitals Authority Youth Programme (QML20230806). We thank L. Bai, R. Bai, J. Lu, J. Chen, Y. Yang, and X. Li for their administrative assistance, Y. Jing and C. Wang for their help in cell culture, J. Jia and F. Liu for their help in animal experiments, J. Jia and Y. Deng for their help with FACS experiments. J. Wang for his help in LC-MS/MS.

Supporting information

The supporting information is available online at https://doi.org/10.1007/s11427-023-2451-3. The supporting materials are published as submitted, without typesetting or editing. The responsibility for scientific accuracy and content remains entirely with the authors.

References

Atlas, A. (2021). Aging Atlas: a multi-omics database for aging biology. Nucleic Acids Res 49, D825–D830.

Bao, H., Cao, J., Chen, M., Chen, M., Chen, W., Chen, X., Chen, Y., Chen, Y., Chen, Y., Chen, Z., et al. (2023). Biomarkers of aging. Sci China Life Sci 66, 893–1066.

Bi, S., Liu, Z., Wu, Z., Wang, Z., Liu, X., Wang, S., Ren, J., Yao, Y., Zhang, W., Song, M., et al. (2020). SIRT7 antagonizes human stem cell aging as a heterochromatin stabilizer. Protein Cell 11, 483–504.

Cai, N., Li, M., Qu, J., Liu, G.H., and Izpisua Belmonte, J.C. (2012). Post-translational modulation of pluripotency. J Mol Cell Biol 4, 262–265.

Cai, W., and Yang, H. (2016). The structure and regulation of Cullin 2 based E3 ubiquitin ligases and their biological functions. Cell Div 11, 7.

Cai, Y., Song, W., Li, J., Jing, Y., Liang, C., Zhang, L., Zhang, X., Zhang, W., Liu, B., An, Y., et al. (2022). The landscape of aging. Sci China Life Sci 65, 2354–2454.

Chai, Z., Sarcevic, B., Mawson, A., and Toh, B.H. (2001). SET-related cell division autoantigen-1 (CDA1) arrests cell growth. J Biol Chem 276, 33665–33674.

Chen, J., Ou, Y., Yang, Y., Li, W., Xu, Y., Xie, Y., and Liu, Y. (2018). KLHL22 activates amino-acid-dependent mTORC1 signalling to promote tumorigenesis and ageing. Nature 557, 585–589.

Chen, T., Chen, X., Zhang, S., Zhu, J., Tang, B., Wang, A., Dong, L., Zhang, Z., Yu, C., Sun, Y., et al. (2021). The genome sequence archive family: toward explosive data growth and diverse data types. Genomics Proteomics Bioinformatics 19, 578–583.

Chen, T., Ma, J., Liu, Y., Chen, Z., Xiao, N., Lu, Y., Fu, Y., Yang, C., Li, M., Wu, S., et al. (2022). iProX in 2021: connecting proteomics data sharing with big data. Nucleic Acids Res 50, D1522–D1527.

Choppara, S., Ganga, S., Manne, R., Dutta, P., Singh, S., and Santra, M.K. (2018). The SCFFBXO46 ubiquitin ligase complex mediates degradation of the tumor suppressor FBXO31 and thereby prevents premature cellular senescence. J Biol Chem 293, 16291–16306.

Consortium, A.B., Zhang, L., Guo, J., Liu, Y., Sun, S., Liu, B., Yang, Q., Tao, J., Tian, X. L., Pu, J., et al. (2023). A framework of biomarkers for vascular aging: A consensus statement by the Aging Biomarker Consortium. Life Med doi: 10.1093/lifemedi/lnad033.

Deng, L., Ren, R., Liu, Z., Song, M., Li, J., Wu, Z., Ren, X., Fu, L., Li, W., Zhang, W., et al. (2019). Stabilizing heterochromatin by DGCR8 alleviates senescence and osteoarthritis. Nat Commun 10, 3329.

Dikic, I. (2017). Proteasomal and autophagic degradation systems. Annu Rev Biochem 86, 193–224.

Dobin, A., Davis, C.A., Schlesinger, F., Drenkow, J., Zaleski, C., Jha, S., Batut, P., Chaisson, M., and Gingeras, T.R. (2013). STAR: ultrafast universal RNA-seq aligner. Bioinformatics 29, 15–21.

Duda, D.M., Borg, L.A., Scott, D.C., Hunt, H.W., Hammel, M., and Schulman, B.A. (2008). Structural insights into NEDD8 activation of Cullin-RING ligases: conformational control of conjugation. Cell 134, 995–1006.

Epping, M.T., Lunardi, A., Nachmani, D., Castillo-Martin, M., Thin, T.H., Cordon-Cardo, C., and Pandolfi, P.P. (2015). TSPYL2 is an essential component of the REST/NRSF transcriptional complex for TGFβ signaling activation. Cell Death Differ 22, 1353–1362.

Fu, L., Hu, Y., Song, M., Liu, Z., Zhang, W., Yu, F.X., Wu, J., Wang, S., Izpisua Belmonte, J.C., Chan, P., et al. (2019). Up-regulation of FOXD1 by YAP alleviates senescence and osteoarthritis. PLoS Biol 17, e3000201.

Geng, L., Zhang, B., Liu, H., Wang, S., Cai, Y., Yang, K., Zou, Z., Jiang, X., Liu, Z., Li, W., et al. (2023). A comparative study of metformin and nicotinamide riboside in alleviating tissue aging in rats. Life Med 2, lnac045.

He, Y., Ji, Q., Wu, Z., Cai, Y., Yin, J., Zhang, Y., Zhang, S., Liu, X., Zhang, W., Liu, G. H., et al. (2023). 4E-BP1 counteracts human mesenchymal stem cell senescence via maintaining mitochondrial homeostasis. Protein Cell 14, 202–216.

Hershko, A., and Ciechanover, A. (1992). The ubiquitin system for protein degradation. Annu Rev Biochem 61, 761–807.

Hipp, M.S., Kasturi, P., and Hartl, F.U. (2019). The proteostasis network and its decline in ageing. Nat Rev Mol Cell Biol 20, 421–435.

Hua, Z., and Vierstra, R.D. (2011). The Cullin-RING ubiquitin-protein ligases. Annu Rev Plant Biol 62, 299–334.

Huang, D., Zuo, Y., Zhang, C., Sun, G., Jing, Y., Lei, J., Ma, S., Sun, S., Lu, H., Zhang, X., et al. (2022). A single-nucleus transcriptomic atlas of primate testicular aging reveals exhaustion of the spermatogonial stem cell reservoir and loss of Sertoli cell homeostasis. Protein Cell doi: 10.1093/procel/pwac057.

Jia, L., Li, H., and Sun, Y. (2011). Induction of p21-dependent senescence by an NAE inhibitor, MLN4924, as a mechanism of growth suppression. Neoplasia 13, 561–569.

Johmura, Y., Harris, A.S., Ohta, T., and Nakanishi, M. (2020). FBXO22, an epigenetic multiplayer coordinating senescence, hormone signaling, and metastasis. Cancer Sci 111, 2718–2725.

Kubben, N., Zhang, W., Wang, L., Voss, T.C., Yang, J., Qu, J., Liu, G.H., and Misteli, T. (2016). Repression of the antioxidant NRF2 pathway in premature aging. Cell 165, 1361–1374.

Langmead, B., and Salzberg, S.L. (2012). Fast gapped-read alignment with Bowtie 2. Nat Methods 9, 357–359.

Lei, J., Jiang, X., Huang, D., Jing, Y., Yang, S., Geng, L., Yan, Y., Zheng, F., Cheng, F., Zhang, W., et al. (2023). Human ESC-derived vascular cells promote vascular regeneration in a HIF-1α dependent manner. Protein Cell doi: 10.1093/procel/pwad027.

Li, L.Z., Yang, K., Jing, Y., Fan, Y., Jiang, X., Wang, S., Liu, G.H., Qu, J., Ma, S., and Zhang, W. (2023). CRISPR-based screening identifies *XPO7* as a positive regulator of senescence. Protein Cell 14, 623–628.

Li, Z., and Xiong, Y. (2017). Cytoplasmic E3 ubiquitin ligase CUL9 controls cell proliferation, senescence, apoptosis and genome integrity through p53. Oncogene 36, 5212–5218.

Liang, C., Liu, Z., Song, M., Li, W., Wu, Z., Wang, Z., Wang, Q., Wang, S., Yan, K., Sun, L., et al. (2021). Stabilization of heterochromatin by CLOCK promotes stem cell rejuvenation and cartilage regeneration. Cell Res 31, 187–205.

Liao, Y., Smyth, G.K., and Shi, W. (2014). featureCounts: an efficient general purpose program for assigning sequence reads to genomic features. Bioinformatics 30, 923–930.

Lin, H.C., Yeh, C.W., Chen, Y.F., Lee, T.T., Hsieh, P.Y., Rusnac, D.V., Lin, S.Y., Elledge, S.J., Zheng, N., and Yen, H.C.S. (2018). C-terminal end-directed protein elimination by CRL2 ubiquitin ligases. Mol Cell 70, 602–613.e3.

Lin, J.J., Milhollen, M.A., Smith, P.G., Narayanan, U., and Dutta, A. (2010). NEDD8-targeting drug MLN4924 elicits DNA rereplication by stabilizing Cdt1 in S phase, triggering checkpoint activation, apoptosis, and senescence in cancer cells. Cancer Res 70, 10310–10320.

Liu, H., Peng, L., So, J., Tsang, K.H., Chong, C.H., Mak, P.H.S., Chan, K.M., and Chan, S.Y. (2019). TSPYL2 regulates the expression of EZH2 target genes in neurons. Mol

Neurobiol 56, 2640–2652.
Liu, X., Liu, Z., Wu, Z., Ren, J., Fan, Y., Sun, L., Cao, G., Niu, Y., Zhang, B., Ji, Q., et al. (2023). Resurrection of endogenous retroviruses during aging reinforces senescence. Cell 186, 287–304.e26.
López-Otín, C., Blasco, M.A., Partridge, L., Serrano, M., and Kroemer, G. (2023). Hallmarks of aging: An expanding universe. Cell 186, 243–278.
Love, M.I., Huber, W., and Anders, S. (2014). Moderated estimation of fold change and dispersion for RNA-seq data with DESeq2. Genome Biol 15, 550.
Magni, M., Buscemi, G., Maita, L., Peng, L., Chan, S.Y., Montecucco, A., Delia, D., and Zannini, L. (2019). TSPYL2 is a novel regulator of SIRT1 and p300 activity in response to DNA damage. Cell Death Differ 26, 918–931.
Noormohammadi, A., Calculli, G., Gutierrez-Garcia, R., Khodakarami, A., Koyuncu, S., and Vilchez, D. (2018). Mechanisms of protein homeostasis (proteostasis) maintain stem cell identity in mammalian pluripotent stem cells. Cell Mol Life Sci 75, 275–290.
Okumura, F., Matsuzaki, M., Nakatsukasa, K., and Kamura, T. (2012). The role of elongin BC-containing ubiquitin ligases. Front Oncol 2, 10.
Pan, H., Cai, N., Li, M., Liu, G., and Izpisua Belmonte, J.C. (2013). Autophagic control of cell 'stemness'. EMBO Mol Med 5, 327–331.
Pan, H., Guan, D., Liu, X., Li, J., Wang, L., Wu, J., Zhou, J., Zhang, W., Ren, R., Zhang, W., et al. (2016). SIRT6 safeguards human mesenchymal stem cells from oxidative stress by coactivating NRF2. Cell Res 26, 190–205.
Petroski, M.D., and Deshaies, R.J. (2005). Function and regulation of Cullin-RING ubiquitin ligases. Nat Rev Mol Cell Biol 6, 9–20.
Ren, X., Hu, B., Song, M., Ding, Z., Dang, Y., Liu, Z., Zhang, W., Ji, Q., Ren, R., Ding, J., et al. (2019). Maintenance of nucleolar homeostasis by CBX4 alleviates senescence and osteoarthritis. Cell Rep 26, 3643–3656.e7.
Sarikas, A., Hartmann, T., and Pan, Z.Q. (2011). The cullin protein family. Genome Biol 12, 220.
Scheffner, M., Nuber, U., and Huibregtse, J.M. (1995). Protein ubiquitination involving an E1-E2-E3 enzyme ubiquitin thioester cascade. Nature 373, 81–83.
Soucy, T.A., Smith, P.G., Milhollen, M.A., Berger, A.J., Gavin, J.M., Adhikari, S., Brownell, J.E., Burke, K.E., Cardin, D.P., Critchley, S., et al. (2009). An inhibitor of NEDD8-activating enzyme as a new approach to treat cancer. Nature 458, 732–736.
Tao, K.P., Fong, S.W., Lu, Z., Ching, Y.P., Chan, K.W., and Chan, S.Y. (2011). TSPYL2 is important for G1 checkpoint maintenance upon DNA damage. PLoS ONE 6, e21602.
Toh, B.H., Tu, Y., Cao, Z., Cooper, M.E., and Chai, Z. (2010). Role of cell division autoantigen 1 (CDA1) in cell proliferation and fibrosis. Genes 1, 335–348.
Tsang, K.H., Lai, S.K., Li, Q., Yung, W.H., Liu, H., Mak, P.H.S., Ng, C.C.P., McAlonan, G., Chan, Y.S., and Chan, S.Y. (2014). The nucleosome assembly protein TSPYL2 regulates the expression of NMDA receptor subunits GluN2A and GluN2B. Sci Rep 4, 3654.
Tu, Y., Wu, T., Dai, A., Pham, Y., Chew, P., de Haan, J.B., Wang, Y., Toh, B.H., Zhu, H., Cao, Z., et al. (2011). Cell division autoantigen 1 enhances signaling and the profibrotic effects of transforming growth factor-β in diabetic nephropathy. Kidney Int 79, 199–209.
Tu, Y., Wu, W., Wu, T., Cao, Z., Wilkins, R., Toh, B.H., Cooper, M.E., and Chai, Z. (2007). Antiproliferative autoantigen CDA1 transcriptionally up-regulates $p21^{Waf1/Cip1}$ by activating p53 and MEK/ERK1/2 MAPK pathways. J Biol Chem 282, 11722–11731.
Wang, C., Yang, K., Liu, X., Wang, S., Song, M., Belmonte, J.C.I., Qu, J., Liu, G.H., and Zhang, W. (2023). MAVS antagonizes human stem cell senescence as a mitochondrial stabilizer. Research 6, 0192.
Wang, K., and Liu, X. (2022). Determining the effects of neddylation on Cullin-RING ligase-dependent protein ubiquitination. Curr Protocols 2, e401.
Wang, Q., Li, H., Tajima, K., Verkerke, A.R.P., Taxin, Z.H., Hou, Z., Cole, J.B., Li, F., Wong, J., Abe, I., et al. (2022a). Post-translational control of beige fat biogenesis by PRDM16 stabilization. Nature 609, 151–158.
Wang, S., Wang, G., Lu, S., Zhang, J., Zhang, W., Han, Y., Cai, X., Zhuang, Y., Pu, F., Yan, X., et al. (2022b). Proteome expression profiling of red blood cells during the tumorigenesis of hepatocellular carcinoma. PLoS ONE 17, e0276904.
Wiśniewski, J.R., Zougman, A., Nagaraj, N., and Mann, M. (2009). Universal sample preparation method for proteome analysis. Nat Methods 6, 359–362.
Xu, X., Sarikas, A., Dias-Santagata, D.C., Dolios, G., Lafontant, P.J., Tsai, S.C., Zhu, W., Nakajima, H., Nakajima, H.O., Field, L.J., et al. (2008). The CUL7 E3 ubiquitin ligase targets insulin receptor substrate 1 for ubiquitin-dependent degradation. Mol Cell 30, 403–414.
Yan, P., Li, Q., Wang, L., Lu, P., Suzuki, K., Liu, Z., Lei, J., Li, W., He, X., Wang, S., et al. (2019). FOXO3-engineered human ESC-derived vascular cells promote vascular protection and regeneration. Cell Stem Cell 24, 447–461.e8.
Yan, P., Ren, J., Zhang, W., Qu, J., and Liu, G.H. (2020). Protein quality control of cell stemness. Cell Regen 9, 22.
Zhang, B., Yan, H., Liu, X., Sun, L., Ma, S., Wang, S., Qu, J., Liu, G.H., and Zhang, W. (2023). SenoIndex: S100A8/S100A9 as a novel aging biomarker. Life Med 2, lnad022.
Zhang, S., Wu, Z., Shi, Y., Wang, S., Ren, J., Yu, Z., Huang, D., Yan, K., He, Y., Liu, X., et al. (2022a). FTO stabilizes MIS12 and counteracts senescence. Protein Cell 13, 954–960.
Zhang, Y., Liu, X., Klionsky, D.J., Lu, B., and Zhong, Q. (2022b). Manipulating autophagic degradation in human diseases: from mechanisms to interventions. Life Med 1, 120–148.
Zhao, H., Ji, Q., Wu, Z., Wang, S., Ren, J., Yan, K., Wang, Z., Hu, J., Chu, Q., Hu, H., et al. (2022). Destabilizing heterochromatin by APOE mediates senescence. Nat Aging 2, 303–316.
Zhou, Y., Zhou, B., Pache, L., Chang, M., Khodabakhshi, A.H., Tanaseichuk, O., Benner, C., and Chanda, S.K. (2019). Metascape provides a biologist-oriented resource for the analysis of systems-level datasets. Nat Commun 10, 1523.
Zhu, J., An, Y., Wang, X., Huang, L., Kong, W., Gao, M., Wang, J., Sun, X., Zhu, S., and Xie, Z. (2022). The natural product rotundic acid treats both aging and obesity by inhibiting PTP1B. Life Med 1, 372–386.
Zimmerman, E.S., Schulman, B.A., and Zheng, N. (2010). Structural assembly of cullin-RING ubiquitin ligase complexes. Curr Opin Struct Biol 20, 714–721.